MINISTRY OF INDUSTRY AND TRADE
INDUSTRIAL UNIVERSITY OF HO CHI MINH CITY

PHAM HOANG AI LE

SYNTHESIS, CHARACTERIZATION AND APPLICATION OF BISMUTH-BASED MOFS

SUMMARY OF DOCTORALE THESIS

DRAFT

Ho Chi Minh City, 2025

MINISTRY OF INDUSTRY AND TRADE
INDUSTRIAL UNIVERSITY OF HO CHI MINH CITY

PHAM HOANG AI LE

SYNTHESIS, CHARACTERIZATION AND APPLICATION OF BISMUTH-BASED MOFS

Specialization: Chemical Engineering
Specialization Code: 9520301

Independent Reviewer 1:

Independent Reviewer 2:

Reviewer 1:

Reviewer 2:

Reviewer 3:

Supervior:

1. Assoc. Prof. Dr. Nguyen Van Cuong
2. Dr. Nguyen Duy Trinh

DRAFT

INTRODUCTION

1. Criticality

In recent decades, the presence of organic pollutants in water media, particularly organic dyes and antibiotics from chemical and pharmaceutical industries, has posed a serious threat to both environment and human health. Consequently, various treatment methods, such as adsorption, coagulation, oxidation-reduction, and photocatalysis, has been developed to mitigate these contaminants. Among these approaches, photocatalysis is recognized as one of the most efficient methods, driving the imperative for continued innovation in photocatalytic materials.

Metal-Organic Framework (MOF) materials have garnered siginificant attention as photocatalysts for the degradation of organic pollutants due to their ability to absorb light and generate excited electron-hole pairs via metal-ligand bonds. Specifically, bismuth-based MOFs (Bi-MOF) offer outstanding advantages, including exceptional light absorption capabilities enabled by their unique three-dimensional structure and large surface area. Bi clusters, linked to organic molecules, form networks that can be tailored to enhance photocatalytic performance. Furthermore, the physicochemical properties of Bi-MOF can be finely tuned by modifying their composition, size, and shape to meet specific application needs. However, their photocatalytic efficiency remains limited due to factors such as extended reaction times and operation predominantly in the UV light region, as result of their bandgap energy (3.3–3.6 eV). Additionally, in single-phase photocatalyst, the recombination of e^-/h^+ further decreases efficiency. To address these challenges, intensive research into the Bi-MOF structure, properties, and applications is essential. A growing area of focus involves incorporating MOF materials as inorganic semiconductors to form heterojunctions. thereby enhancing photocatalytic efficiency and expanding their practical applications.

This dissertation focuses on the synthesis of new photocatalysts based on Bi-MOF, including Bi-MOF heterojunction systems and related materials, and their application in the degradation of organic pollutants. The results presented herein contribute both theoretical insights and practical advancements to the field of photocatalysis using bismuth-based MOF materials, promoting the development of future applications for Bi-MOF materials.

2. Research objectives

Bismuth-based MOFs and their composite systems are synthesized and characterized, focusing on optimizing their structural, optical, and physicochemical properties for photocatalytic applications.

3. Research subjects

Bi-MOF materials, based on bismuth metal centers and organic linkers like H_2BDC and H_3BTC, were investigated. Composites containing Bi-MOF, such as the CAU-17/BiOCl composite system and BiOCl/BHP derived from CAU-17, were also explored. Organic compounds, including dyes such as rhodamine B (RhB) and antibiotics like tetracycline (TC) and sulfamethoxazole (SMX), were used as model pollutants to evaluate the photocatalytic activity of the synthesized catalysts.

4. Research content

- BiBDC metal-organic framework material was synthesized from bismuth metal centers and the organic linker H_2BDC. CAU-17, UU-200, and MIX-UCAU were synthesized using bismuth metal centers and the organic linker H_3BTC. Heterojunction composites containing

DRAFT

Bi-MOF, such as the CAU-17/BiOCl and BiOCl/BHP derived from CAU-17 were also synthesized.

- The synthesized materials were characterized using a variety of techniques,such as XRD, FT-IR, SEM, TEM, XPS, BET, UV-Vis DRS, EIS, and PL.

- The photocatalytic activity of BiBDC, BiBTC, CAU-17/BiOCl, and BiOCl/BHP materials was evaluated for the degradation of organic pollutants such as RhB, TC, and SMX.

5. Scientific and practical significance

- Scientific Significance: The synthesis and characterization of these materials contribute to building a comprehensive database of bismuth-based metal-organic framework materials and Bi-MOF composites, thus advancing the field of photocatalysis and material science.

- Practical Significance: Photocatalytic materials play a crucial role in the degradation of organic pollutants, significantly contributing to environmental protection and public health by mitigating harmful contaminants in water and air.

6. Research novelty

Successful synthesis of bismuth-terephthalate (BiBDC) metal-organic frameworks using the solvothermal method at varying temperatures. The synthesis temperature significantly influences the morphology, crystallinity, bandgap energy, and photocatalytic activity of BiBDC materials.

Successful integration of UU-200 and CAU-17 metal-organic frameworks into MIX-UCAU materials. The resultant integrated MOF exhibited enhanced photophysical properties and improved charge separation efficiency compared to individual MOFs. These enhancements led to a a substantial increase in the photocatalytic degradation efficiency of RhB.

A CAU-17/BiOCl heterojunction system was successfully synthesized, combining a metal-organic framework with an inorganic semiconductor. This was achieved through the direct solvothermal growth of CAU-17 on flower-like BiOCl nanosheets. The CAU-17/BiOCl material demonstrated high efficiency in degrading RhB and TC. A photocatalytic mechanism based on the S-scheme heterojunction model was proposed to explain the observed activity.

Successful synthesis of the BiOCl/BHP heterojunction system derived from the CAU-17 metal-organic framework. The BiOCl/BHP material featured an optimized surface, facilitating enhanced charge separation and transfer processes. This heterojunction demonstrated effective photocatalytic activity for degrading RhB and SMX. The S-scheme heterojunction model was also proposed as the underlying mechanism for the photocatalytic performance of this system.

DRAFT

CHAPTER 1: INTRODUCTION

1.1. Metal-Organic Frameworks (MOFs)

MOFs are a class of materials composed of metal ions coordinated with organic linkers, characterized by their unique structures, diverse properties, and extensive applications. MOFs are typically synthesized through solvothermal or hydrothermal methods, with synthesis parameters such as precursors selection, temperature, pressure, and reaction time playing critical role in determining their structure and performance. The choice of organic linkers and metal ions plays is particularly significant, as it directly influences the physicochemical properties and potential applications of these materials.

1.2. Bismuth-Based Metal-Organic Frameworks

Bismuth (Bi) exhibits a strong affinity for negatively charged bonds, enabling the formation of stable complexes with organic linkers. Bismuth-based metal-organic frameworks (Bi-MOFs) have attracted attention due to their structural stability, environmental compatibility, and versatile applications. To date, approximately 10 porous Bi-MOF materials have been reported, including CAU-7, NOTT-220, CAU-17, CAU-33, Bi-NU-901, SU-100, Bi-TBAPy-2, and SU-101. These frameworks are significant in the fields of chemistry and materials science.

Research indicates that the photocatalytic efficiency of Bi-based MOFs can be tuned by altering synthesis parameters such as the choice of organic linkers, temperature, time, pH, and the use of catalysts additives. Additionally, Bi-MOF materials can be integrated with inorganic semiconductors like BiOCl to form composites. These composite exhibit enhanced photocatalytic performance due to improved electron separation and efficient charge transfer processes. Such advancements facilitate the degradation of organic pollutants under sunlight irradiation, making Bi-MOF composites promising candidates for water treatment applications. Moreover, there is an increasing focus on converting Bi-MOFs into inorganic semiconductors such as BiOCl and BHP, to achieve superior efficiency and durability in photocatalytic processes. This approach may broaden the scope of Bi-MOFs in addressing environmental challenges and advancing sustainable technologies.

1.3. BiOCl material

BiOCl is a layered material characterized by strong covalent bonds within its $[Bi_2O_2]^{2+}$ layers, which are interspersed with adjacent Cl^- layers. The Cl^- layers are connected by weaker van der Waals forces, contributing to the overall structure of BiOCl. BiOCl typically exhibits a sheet-like crystalline morphology and appears white or pale in color. As a semiconductor, BiOCl possesses excellent light absorption properties, making it a promising candidate for photocatalytic applications.

1.4. BHP materials (Bismuth-based halide perovskites)

Bismuth-based halide perovskites (BHP) are hybrid materials with a perovskite crystal structure, typically represented by the general formulas ABX_3 or $A_3B_2X_9$. In these structures, A represents a large cation, such as organic cation methylammonium (MA^+), formamidinium (FA^+), or inorganic cations like cesium (Cs^+) and methylammonium ($CH_3NH_3^+$). X is a halide anion, including chloride (Cl^-), bromide (Br^-), or iodide (I^-). The perovskite structure of BHP can be finely tailored by altering the A, B, and X components, allowing precise control over its physical and chemical properties. The layered architecture of BHP endows it with remarkable features, including efficient light absorption, tunable bandgap energies, and compositional flexibility. These characteristics make BHP a promising material for applications in efficient photocatalysis.

1.5. Methods to Enhance the Photocatalytic Efficiency of Heterojunction Systems

DRAFT

When two semiconductors with distinct energy band structures are coupled, an interface forms a heterojunction. The construction of heterojunctions has been shown to significantly improve photocatalytic efficiency. Key attributes of heterojunctions include extending the optical absorption range, enhancing the separation and movement of charge carriers, and improving chemical stability. These factors collectively contribute to increased photocatalytic performance.

Heterojunctions can be classified into four types: traditional, p-n, Z-scheme, and S-scheme. The traditional heterojunction is formed by coupling two semiconductors through a standard electronic transition process, which increases catalytic efficiency but still exhibits relatively inefficient electron-hole pair separation. The p-n heterojunction is established by combining p-type (hole-rich) and n-type (electron-rich) semiconductors, where the internal electric field at the interface enhances electrons-holes separation, thus improving photocatalytic efficiency. The Z-scheme heterojunction features a structure that facilitates indirect electron transfer, while preserving the robust oxidation and reduction capabilities of the semiconductors, resulting in superior photocatalytic performance. The S-scheme, an advanced variation of the Z-scheme, offers even more efficient charge carriers separation, leading to a substantial improvement in photocatalytic efficiency.

1.6. Overview of Organic Pollutants

Organic pollutants in water not only adversely affect the aquatic environment but also pose serious risks to human health. Various methods have been employed to reduce the concentration of pollutants, including adsorption, coagulation, biological treatment, and advanced oxidation. Among these, photocatalytic degradation of organic pollutants has emerged as a particularly advantageous approach due to its high treatment efficiency, capacity to completely mineralize harmful organic compounds into less toxic inorganic substances, and widespread application in environmental remediation. Therefore, the research and development of advanced photocatalytic materials are of critical importance. Bi-MOFs and their composites have demomstrated significant potential as photocatalysts for enhancing the degradation of organic pollutants.

The objective of this dissertation is to improve the photocatalytic efficiency of metal-organic frameworks based on bismuth metal centers by systematically investigating synthesis parameters, including reaction temperature and the selection of organic linkers for Bi-MOFs (Figure 1.1). Additionally, the study aims to develop heterojunctions of Bi-MOFs with BiOCl and BHP materials. These heterojunction are designed to reduce bandgap energy, prevent the recombination of e^-/h^+ pairs, and enhance the degradation efficiency of RhB, TC, and SMX under visible light irradiation.

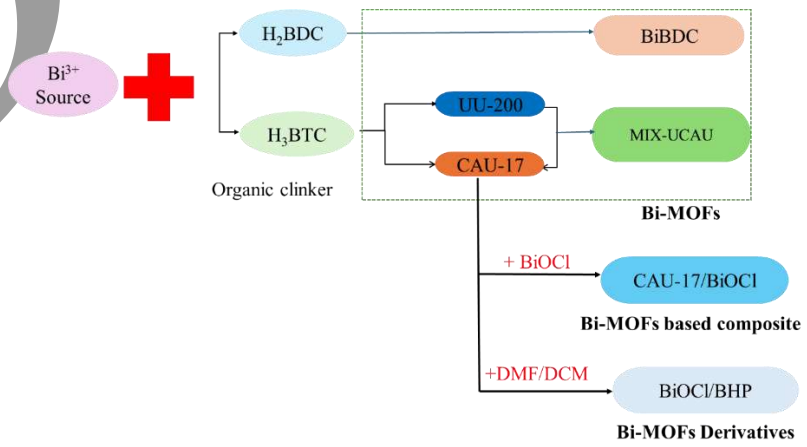


Figure 1.1: Bi-MOF materials, composite systems, and Bi-MOF derivatives studied in the dissertation.

DRAFT

CHAPTER 2: EXPERIMENT METHOD

2.1 Material synthesis

BiBDC was synthesized using a solvothermal method by dissolving $Bi(NO_3)_3 \cdot 5H_2O$ and H_2BDC in DMF. Then, the solution was heated in a Teflon-lined stainless-steel autoclave at 80, 100, or 120 °C for 48 hours. After the reaction, the product was allowed to cool to room temperature, recovered by centrifugation, washed thoroughly with DMF and ethanol, and subsequently dried before further use.

UU-200, CAU-17, and MIX-UCAU were also synthesized via the solvothermal method. For the synthesis of UU-200, $Bi(NO_3)_3 \cdot 5H_2O$ and H_3BTC were dissolved in DMF and heated in a Teflon-lined stainless-steel autoclave at 140 °C for 24 hours. For the synthesis of CAU-17, $Bi(NO_3)_3 \cdot 5H_2O$ and H_3BTC were dissolved in a solvent mixture of MeOH (55 mL) and H_2O (5 mL), and the reaction was conducted at 120 °C for 12 hours in a Teflon-lined stainless-steel autoclave. MIX-UCAU, a hybrid MOF combining UU-200 and CAU-17, was synthesized in a solvent mixture of DMF and MeOH. After the reaction, the products were allowed to cool to room temperature, recovered by centrifugation, washed thoroughly with DMF and ethanol, and subsequently dried before further use.

The CAU-17/BiOCl heterostructure was prepared by anchoring CAU-17 onto BiOCl through a solvothermal reaction conducted at 120 °C for 6, 12, or 24 hours. While, BiOCl/BHP was synthesized from CAU-17 by dispersing 0.5 g of CAU-17 in DMF and DCM. The reaction was carried out at 155 °C for varying durations (1, 4, 8, or 16 hours). The product was collected by centrifugation, washed with DMF, and dried at 80 °C.

2.2 Physical and Chemical Characterization Methods of Materials

The synthesized materials were characterized to determine their crystal structure, thermal properties, surface morphologies, optical characteristics, and electrochemical behaviors. Characterization techniques included XRD, FT-IR, TGA, XPS, SEM-EDX, TEM, BET, UV-Vis DRS, EIS, and PL.

2.3 Evaluation of the catalytic activity of synthesized materials

In this dissertation, the photocatalytic activities of Bi-MOFs and their composites were evaluated through the degradation of organic pollutants, including RhB, TC, and SMX. The photocatalytic reaction system was custom-designed, comprising a double-layered 100 mL glass reactor and a 40W Cree® Xlamp® XM-L2 LED light source. Reaction products were analyzed using a UV-vis spectrophotometer and liquid chromatography coupled with an ion trap detector (Thermo Finnigan LCQ MS, model Agilent 6410 Triple Quad LC/MS/MS). Each photocatalytic experiments were repeated three times, and the mean values along with the corresponding standard deviations were calculated to ensure reproducibility and accuracy.

To determine optimal reaction conditions, the degradation of RhB was systematically investigated by varying key parameters, including catalyst dosage, RhB concentration, and reaction pH. Radical scavenger experiments were conducted to identify the reactive species involved in the photocatalytic process. Specific scavengers were employed, such as p-BQ (1,4-benzoquinone), $Na_2C_2O_4$ (sodium oxalate), $K_2Cr_2O_7$ (potassium dichromate), and tert-butanol (TBA) for trapping $\bullet O_2^-$, h^+, e^-, and •OH radicals, respectively. For each experiment, 5 mL of a 10^{-3} M scavenger solution was added to the photocatalytic reaction under conditions identical to those described in the photocatalytic test mentioned above. Also, the reusability of the catalysts was evaluated to assess their stability and durability over multiple photocatalytic cycles, ensuring the long-term applicability of the as-synthesized photocatalysts.

DRAFT

CHAPTER 3: RESULTS AND DISCUSSION

3.1. Synthesis of BiBDC Material and Its Application as a Photocatalyst for RhB Degradation

3.1.1. Results of the synthesis of BiBDC

The BiBDC was synthesized via a solvothermal reaction between H_2BDC and $Bi(NO_3)_3 \cdot 5H_2O$ using the solvothermal method, as described in Figure 3.1. The synthesis was conducted at various temperatures, resulting in powdered with distinct colors. Specifically, BiBDC synthesized at 80 °C (BiBDC-80) and 100 °C (BiBDC-100) appeared white, whereas BiBDC synthesized at 120 °C (BiBDC-120) exhibited a light grayish-white hue.

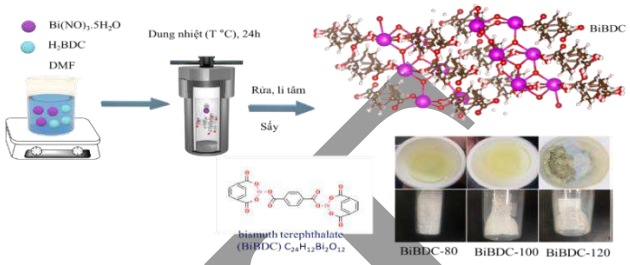


Figure 3.1: BiBDC product synthesized at different temperatures

3.1.2. Results of crystal structure and thermal properties analysis of BiBDC material

The XRD analysis results shown in Figure 3.2 (a) indicate that the synthesized BiBDC material exhibits characteristic diffraction peaks at 2θ values of 7.6°, 9°, 16.6°, and 25.8°, corresponding to bismuth terephthalate with a sheet-like structure (CCDC number 793572). Additionally, when the reaction temperature was increased to 120°C, the BiBDC-120 material shows a decrease in the intensity of the main BiBDC phase peaks, along with the formation of a new phase. Peaks at 27.12°, 37.9°, 39.84°, and 48.62° are observed, corresponding to Bi_2O_3 formation.

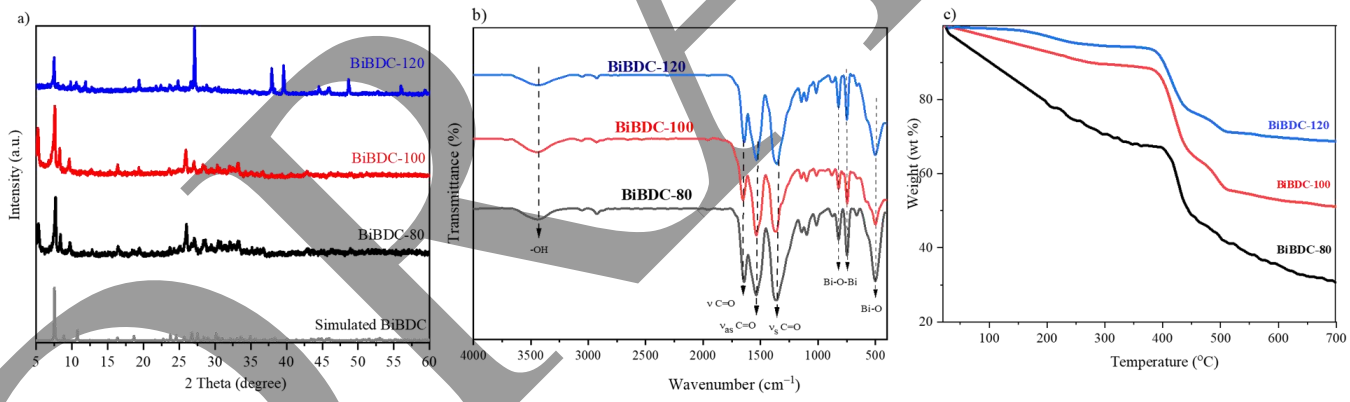


Figure 3.2: (a) XRD Pattern, (b) FT-IR Spectrum, (c) : TGA Analysis of BiBDC

The FT-IR analysis results of the BiBDC material (Figure 3.2 (b)) show characteristic peaks at 1652 cm^{-1} (C=O), 1540 cm^{-1} (asymmetric COO^-), and 1365 cm^{-1} (symmetric COO^-), confirming the presence of functional groups associated with BiBDC. These vibrations are shifted compared to those observed in H_2BDC, indicating the coordination and bonding of Bi^{3+} ions with the functional groups of H_2BDC. In addition, vibrations at approximately 821, 750, and 500 cm^{-1} are attributed to Bi–O–Bi and Bi–O bonds, further confirming the successful formation of the BiBDC framework structure.

The TGA analysis of the BiBDC material, as shown in (Figure 3.2 (c)), reveal an initial weight loss below 100°C, which is attributed to the evaporation of residual solvents. A subsequent weight loss is observed between 100-250°C, corresponding to the release of solvent molecules adsorbed within the pore matrix of material. A significant weight loss occurs around 380°C, corresponding to the decomposition of the organic linker H_2BDC, indicating that the BiBDC material exhibits thermal stability up to 380°C.

DRAFT

3.1.3. Results of surface morphology characterization of the material

The results shown in Figure 3.3 (a-c) indicate notable variations in the crystal morphology of BiBDC at different synthesis temperatures. At 80°C, the BiBDC particles aggregate into large clusters. In contract, when the temperature was increased to 100°C and 120°C, the material transition to a needle-like crystal structure, with individual crystals measuring 2–3 µm in length.

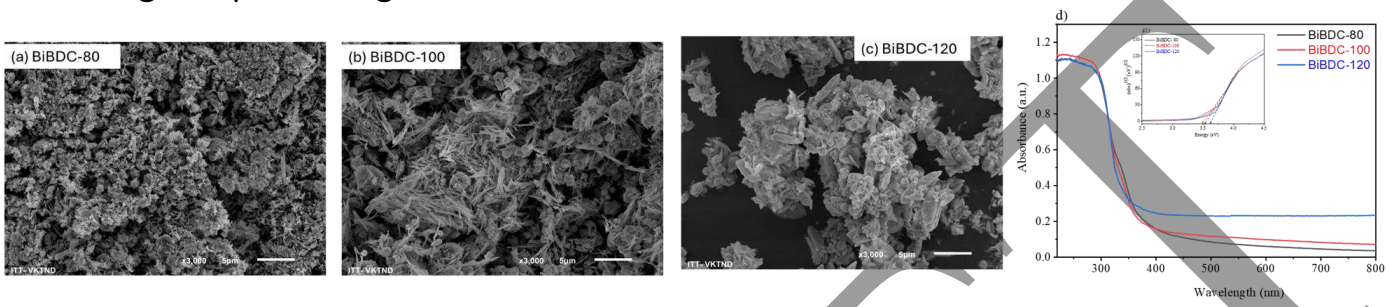


Figure 3.3: (a-c) SEM images of samples, (d) UV-Vis diffuse reflectance spectroscopy spectrum of the BiBDC material

3.1.4. Optical and electrochemical properties of BiBDC material

The optical properties of BiBDC-80, BiBDC-100, and BiBDC-120 materials were investigated using UV-Vis Diffuse Reflectance Spectroscopy (UV-Vis DRS). As shown in Figure 3.3 (d), these materials exhibit an absorption edge in the range of 350–400 nm, indicating their ability to absorb light in the UV-visible region. The bandgap energy (E_g) of BiBDC-80, BiBDC-100, and BiBDC-120 was determined using the Tauc method, as shown in Figure 3.3 (d). The calculated E_g values are 3.58 eV, 3.55 eV, and 3.62 eV, respectively, for BiBDC-80, BiBDC-100, and BiBDC-120, respectively.

3.1.5. RhB Degradation Ability of BiBDC Material

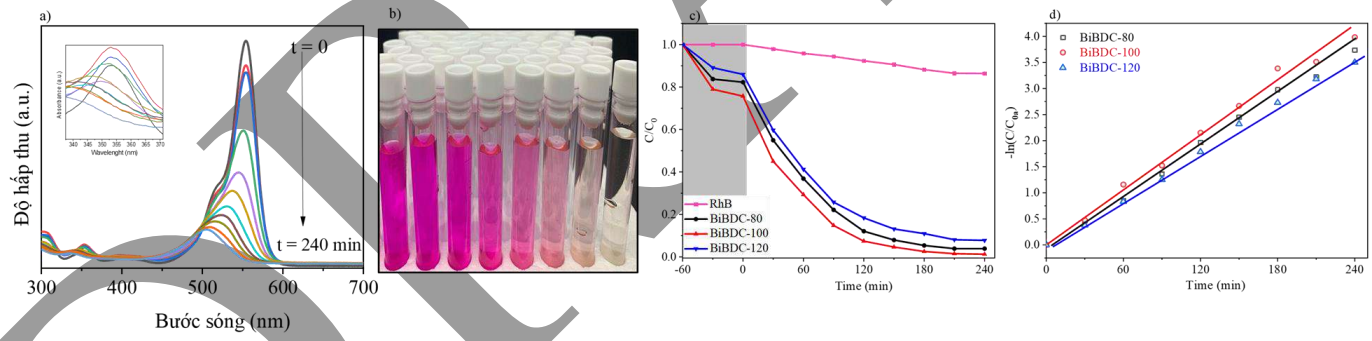


Figure 3.4: (a) Absorption spectrum of RhB solution, (b) Color change of RhB over photocatalytic reaction time, (c) Photocatalytic activity, (d) kinetic equation for RhB degradation of BiBDC.

The results presented in Figure 3.4 indicate that the absorption intensity of RhB decreases over time during the degradation process. The maximum absorption wavelength shifts from 554 nm to 500 nm, which is attributed to the degradation of RhB. Figure 3.4 shows that the adsorption of RhB on the catalyst surface reaches equilibrium after 60 minutes. When BiBDC-100 is used, the degradation efficiency of RhB reaches approximately 98% after 240 minutes of light irradiation, the highest among the BiBDC materials synthesized at 80°C and 120°C. Kinetic studies show that the degradation rate constant for RhB follows the order: BiBDC-100 > BiBDC-80 > BiBDC-120, demonstrating that RhB degrades more rapidly on the BiBDC-100 catalyst.

3.1.6. Factors affecting the photocatalytic activity of BiBDC-100

DRAFT

Figure 3.5 illustrates the influence of various factors, including catalyst amount, pollutant concentration, and pH, on the RhB removal efficiency over the BiBDC-100 catalyst. The efficiency increases with an increased amount of material. A lower initial concentration of RhB leads to faster degradation. An acidic environment improves the photocatalytic reaction efficiency, whereas an alkaline environment reduces the efficiency.

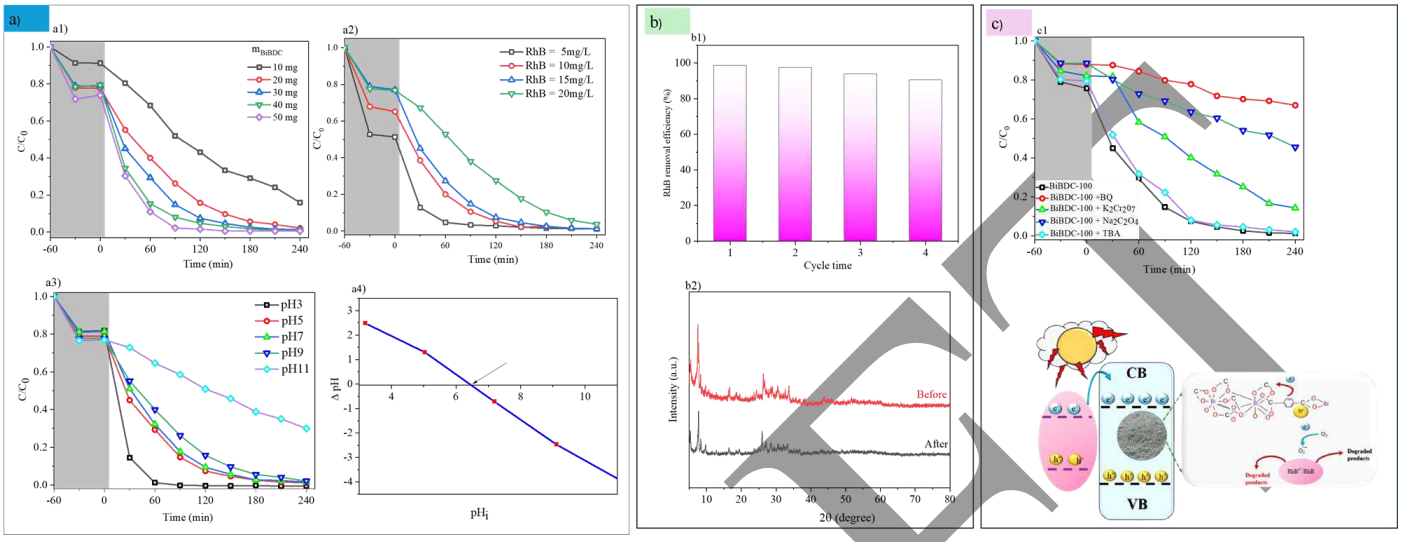


Figure 3.5: (a-) Photocatalytic Activity of BiBDC material for RhB degradation, b) RhB Removal Efficiency upon Reuse of BiBDC-100, (c) Proposed Photocatalytic mechanism on BiBDC-100 material.

The stability of BiBDC-100 under photocatalytic conditions was assessed over 4 cycles of LED light irradiation (Figure 3.5 (b)). After four cycles, there was a slight reduction in the degradation rate of RhB was observed, which can be attributed to the loss of photocatalyst during the washing and experimental process. Besides, the XRD pattern of BiBDC-100 after four cycles of reuse was analyzed (Figure 3.5 (b)). The XRD pattern showed no significant change when compared to that of the fresh photocatalyst, indicating the structural stability of the material after multiple reuse cycles.

3.1.7. Photocatalytic mechanism of BiBDC-100

The results shown in Figure 3.5 (c) indicate that $\bullet O_2^-$, h^+, and e^- radicals are the primarily contributors to the photocatalytic process. The proposed photocatalytic mechanism of BiBDC-100 for RhB degradation is depicted in Figure 3.5. When irradiated, RhB adsorbed on the catalyst surface absorbs light and is excited to the RhB* state. Then, electrons are transferred from the Lowest Unoccupied Molecular Orbital (LUMO) of RhB to the conduction band of the BiBDC-100 material. These electrons then react with O_2 at the catalyst surface to form $^{\bullet}O_2^-$. The generated $^{\bullet}O_2^-$ radicals participate in the oxidation-reduction reactions with RhB/RhB* molecules, leading to their degradation.

The intermediates formed during RhB degradation were identified through LC-MS analysis. The LC-MS spectra,, indicate m/z values of 443, 399, and 355. Based on the LC-MS analysis, the proposed RhB degradation mechanism involves carboxylation, followed by dealkylation and demethylation processes. Ultimately, the intermediates decompose into low-molecular-weight by products, such as CO_2 and H_2O.

The BiBDC, synthesized using bismuth centers and terephthalic acid organic linkers through a solvothermal method, demonstrated that reaction temperature significantly influenced its crystal structure and morphology, thereby enhancing its photocatalytic performance.

3.2. Synthesis of MIX-UCAU Material and Its Application as a Photocatalyst for RhB Degradation

DRAFT

3.2.1. Results of the Synthesis of MIX-UCAU Metal-Organic

Bi-MOFs, including CAU-17, UU-200, and MIX-UCAU (a hybrid of CAU-17 and UU-200), were successfully synthesized using bismuth as the metal center and trimesic acid as the organic linker. The synthesis process for the MIX-UCAU MOF is described in Figure 3.6. The synthesized products UU-200, CAU-17, and MIX-UCAU were obtained as white powders.

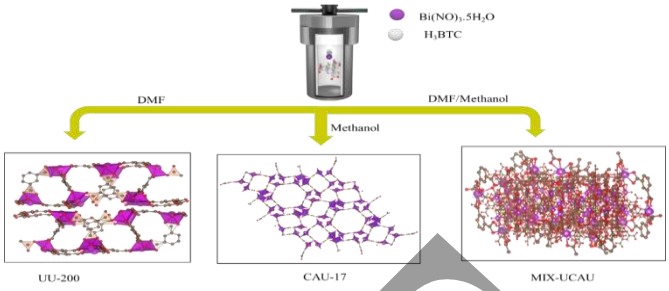


Figure 3.6: Structural Description of UU-200, CAU-17, and MIX-UCAU Materials

3.2.2. Results of Crystal Structure and Thermal Properties Analysis of MIX-UCAU Material

The XRD analysis results (Figure 3.7 (a)) demonstrate the crystal structure of UU-200, CAU-17, MIX-UCAU, and their corresponding simulated models (UU-200: CCDC 2103784, CAU-17: CCDC 1426169). The XRD pattern of UU-200 shows diffraction peaks at 2θ values of 8.11°, 9.45°, 9.79°, 10.28°, and 21.9°, which align with the simulated XRD pattern of UU-200 (CCDC 2103784). In addition, the XRD pattern of CAU-17 shows characteristic peaks at 2θ values of 6.48°, 7.48°, 9.90°, and 13.30°, matching the simulated XRD pattern of CAU-17 (CCDC 1426169). For the MIX-UCAU material, the XRD pattern shows the characteristic diffraction peaks of both UU-200 and CAU-17, meaning that the MIX-UCAU material incorporates the structural features of both MOFs. Notably, the MIX-UCAU material shows higher diffraction peak intensities compared to the individual UU-200 and CAU-17 materials.

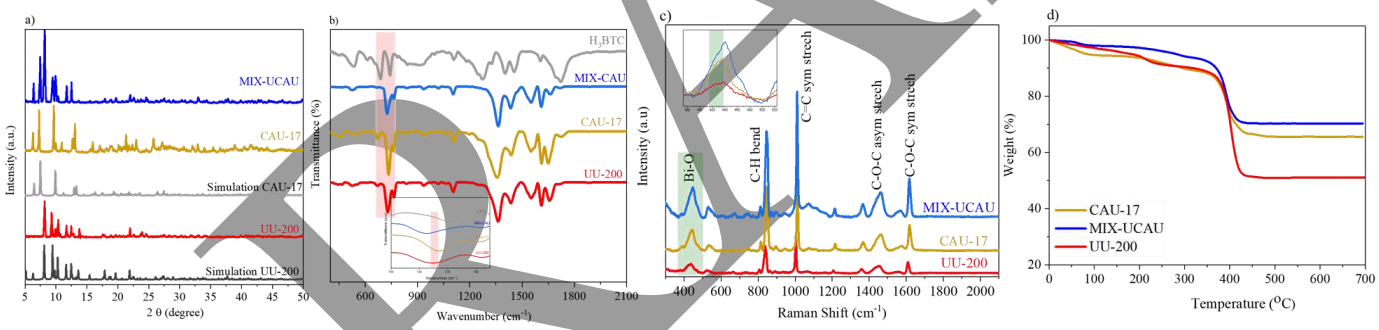


Figure 3.7: (a) XRD Diffraction Pattern, (b) FT-IR Spectrum, (c) Raman Spectrum, (d) TGA Thermal Analysis of CAU-17, UU-200, and MIX-UCAU,

The FT-IR results shown in Figure 3.7 (b) reveal the characteristic functional groups of the synthesized materials. The UU-200, CAU-17, and MIX-UCAU materials show shifts and reductions in the intensity of peaks associated with the functional groups of organic linker H_3BTC, indicating interaction between the organic linker and Bi^{3+} ions. Additionally, a new peak at 527 cm^{-1} is observed, corresponding to the stretching vibration of the Bi–O bond, as well as vibrations associated with C–C, C–O–C bonds. Thermal analysis (Figure 3.7 (d)) shows that the CAU-17, UU-200, and MIX-UCAU materials maintain stability up to approximately 400°C.

XPS analysis (Figure 3.8) provides insights into the chemical composition and oxidation states of the elements C, O, and Bi in the materials CAU-17, UU-200, and MIX-UCAU. The Bi 4f binding energy peaks for Bi^{3+} in the UU-200 sample show a slight shift compared to CAU-17, indicating differences in the way in chemical bond formation or potential changes in the crystal structure. The MIX-UCAU material also exhibits a shift in the Bi 4f peaks due to its integrated structure. The C 1s and O 1s spectra identify the presence of C–C, C–O, C=O,

DRAFT

and Bi–O bonds. The MIX-UCAU material shows a higher content of oxygen defects, which is believed to enhance its photocatalytic performance. These increased oxygen vacancies may facilitate the generation of reactive oxygen species (ROS), thereby improving the photocatalytic activity of catalysts under light irradiation.

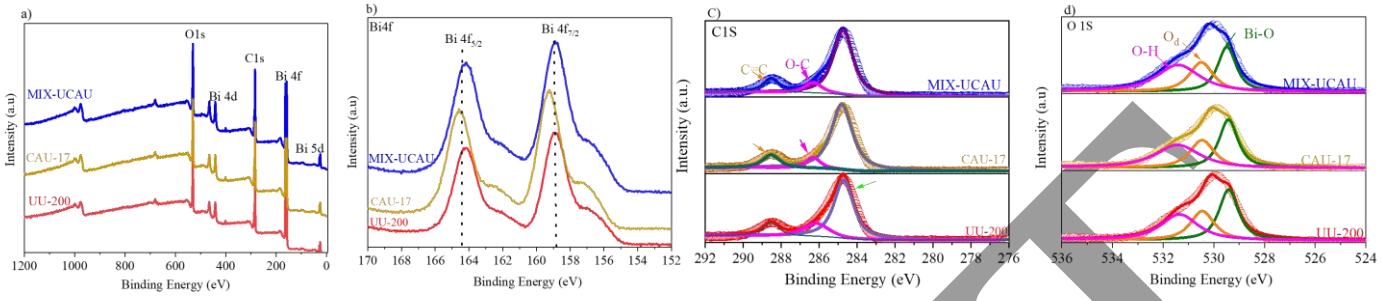


Figure 3.8: (a) General XPS Spectrum of UU-200, CAU-17, and MIX-UCAU, XPS Spectra of (b) Bi 4f, (c) C 1s, and (d) O 1s

3.2.3. Results of surface morphology characterization of MIX-UCAU material

The surface morphology of the as-synthesized materials, as oberved by SEM measurements (Figure 3.9 (a-c)), shows that a rod-like crystal structure with variations in sizes. The UU-200 material exhibits elongated, distinct rod-shaped crystals, whereas CAU-17 shows rod-shaped crystals that tend to aggregate into clusters. The MIX-UCAU material demonstrates a similar morphology to CAU-17 but with shorter crystals that are more tightly aggregated. Furthermore, EDS analysis of the MIX-UCAU sample (Figure 3.9 (d-g)) indicates a highly uniform distribution of Bi, C, and O, confirming are even dispersion of these elements throughout the structure of material.

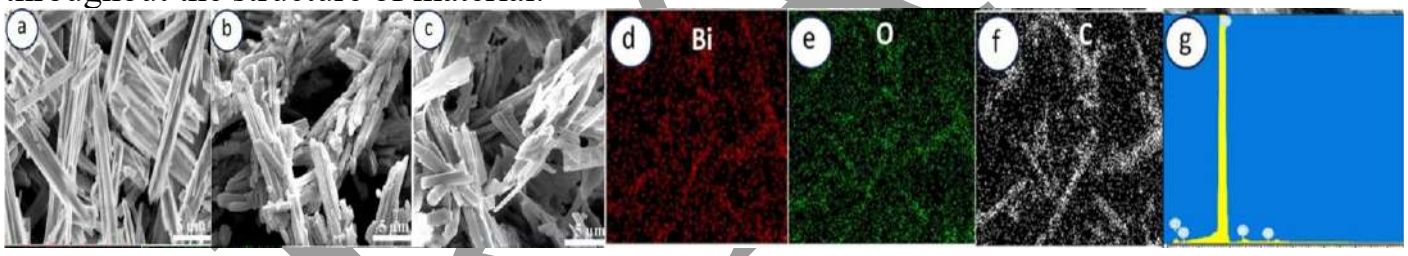


Figure 3.9: (a) SEM Image of UU-200, (b) SEM Image of CAU-17, (c) SEM Image of MIX-UCAU; (d-g) Elemental Distribution Maps of Bi (d), O (e), Carbon (f), (g) EDS Spectrum of MIX-UCAU

3.2.4. Results of Surface Morphology Characterization of MIX-UCAU Material

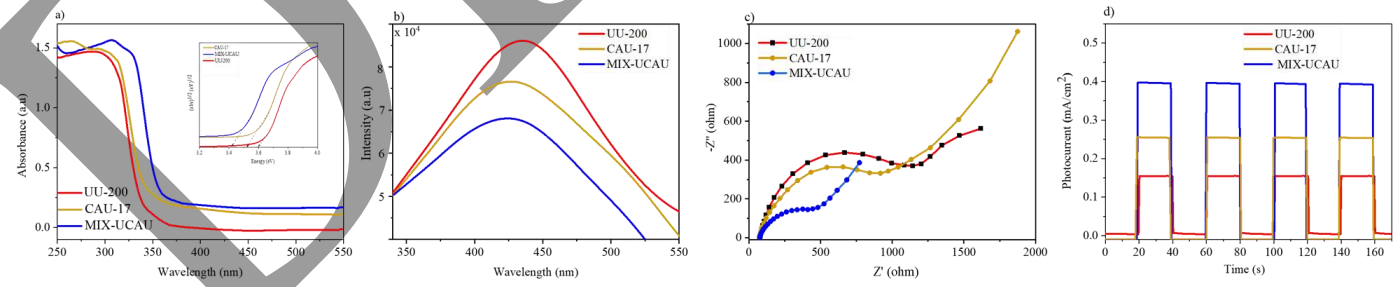


Figure 3.10: Characterization of CAU-17, UU-200, and MIX-UCAU materials:
(a) UV-Vis DRS spectra, with the inset showing the bandgap energy, (b) Photoluminescence (PL) spectra; (c) Electrochemical impedance spectroscopy (EIS) spectra; and (d) Photocurrent response (I-t) over time.

Figure 3.10 presents the optical and electrochemical properties of UU-200, CAU-17, and MIX-UCAU. The UV-Vis DRS of MIX-UCAU (Figure 3.10 a) shows a redshift in the absorption edge, indicating enhanced light absorption capability. The calculated E_g values 3.60 eV for UU-200 and 3.53 eV for CAU-17 , and 3.43 eV for MIX-UCAU, demonstrating that

DRAFT

MIX-UCAU has improved visible light absorption efficiency. In the photoluminescence (PL) analysis (Figure 3.10 b), MIX-UCAU shows the lowest fluorescence peak intensity, which suggests more effective separation of photogenerated charge carriers under light irradiation. Electrochemical impedance spectroscopy (EIS) results (Figure 3.10 c) further confirm the superior charge separation and transfer properties of MIX-UCAU, as evidenced by its reduced charge transfer resistance compared to UU-200 and CAU-17. Moreover, the transient photocurrent response under visible light irradiation (Figure 3.10 d) demonstrates that MIX-UCAU exhibits the highest and most stable photocurrent signal, indicating significant improvement in charge separation and carrier mobility due to its integrated MOF structure.

3.2.5. Photocatalytic Degradation of RhB by MIX-UCAU Material

The results presented in Figure 3.11 show that MIX-UCAU exhibits the highest RhB degradation efficiency, achieving approximately 99% after 90 minutes of light irradiation, compared to 81% for UU-200 and 89% for CAU-17. The superior photocatalytic performance of MIX-UCAU is attributed to the synergistic effect of the combined structures of UU-200 and CAU-17, which leads to the formation of a heterojunction system. This system enhances the separation and mobility of photogenerated electrons and holes, thereby improving the photocatalytic efficiency. The reaction rates for RhB degradation follow the order: MIX-UCAU > CAU-17 > UU-200 > no catalyst, confirming that MIX-UCAU possesses the best photocatalytic activity among the materials studied.

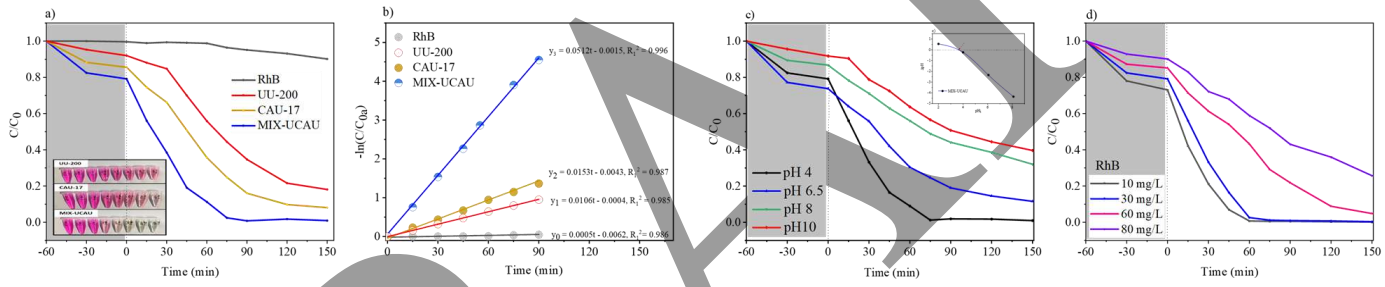


Figure 3.11: Evaluation of photocatalytic performance of CAU 17, UU-200, and MIX-UCAU in RhB degradation; (a) Photocatalytic activity comparison; (b) Kinetic equations for RhB photodegradation using CAU-17, UU-200, and MIX-UCAU catalysts, Photocatalytic Activity of MIX-UCAU for RhB Degradation: (c) Effect of pH, (d) Effect of Initial RhB Concentration

3.2.6. Factors dffecting the degradation of RhB using MIX-UCAU material

The MIX-UCAU material was used to investigate the effects of initial RhB concentration and pH on its photocatalytic degradation efficiency. As shown in Figure 3.11 (c), the degradation efficiency of RhB over MIX-UCAU is strongly influenced by the pH of the reaction medium. At a pH below 6.5, the degradation efficiency reaches 99% within 60 minutes, whereas efficiency decreases at higher pH levels. This dependency on pH is attributed to the electrostatic interactions between the surface of the MIX-UCAU catalyst and the RhB dye molecules, which are more favorable under acidic conditions. Furthermore, as shown in Figure 3.11 (d), RhB is completely degraded within one hour at initial concentrations ranging from 10 to 30 mg/L. However, the degradation efficiency decreases when the concentration increases to 60 mg/L. This reduction in efficiency is due to the saturation of active sites on the catalyst surface and the limited light penetration to the catalyst surface under higher dye concentrations

3.2.7. Reusability of MIX-UCAU material

The stability of the MIX-UCAU material was tested through reuse experiments. The results show that the degradation efficiency of RhB remained approximately 84% after five cycles of use, with only a slight decrease compared to the initial performance. This minor reduction in efficiency may be due to the adsorption of RhB or its intermediate products on

DRAFT

the active sites of the catalyst. Also, SEM images and XRD pattern after/before reaction indicate that MIX-UCAU retains its structural integrity and exhibits good stability after multiple cycles.

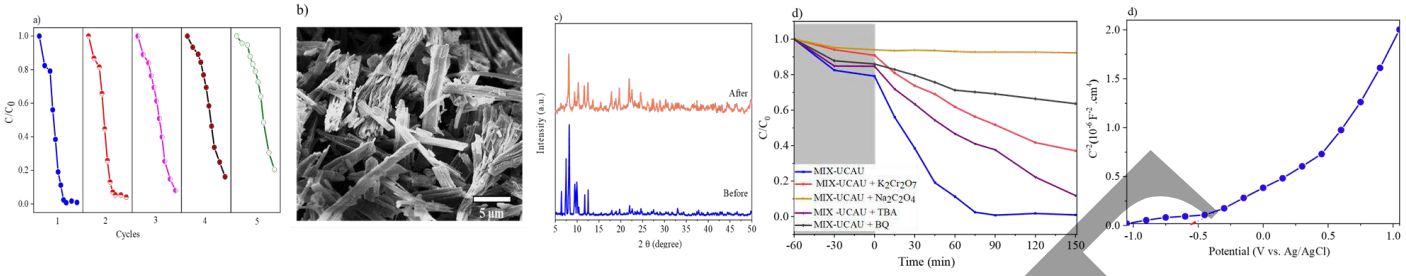


Figure 3.12: (a) RhB degradation efficiency, (b) SEM image, and (c) XRD pattern of MIX-UCAU after reuse, (d) Photocatalytic Activity of MIX-UCAU with Radical Scavengers for RhB Degradation, (e) Mott-Schottky Analysis of MIX-UCAU Material

3.2.8. Photocatalytic mechanism of MIX-UCAU

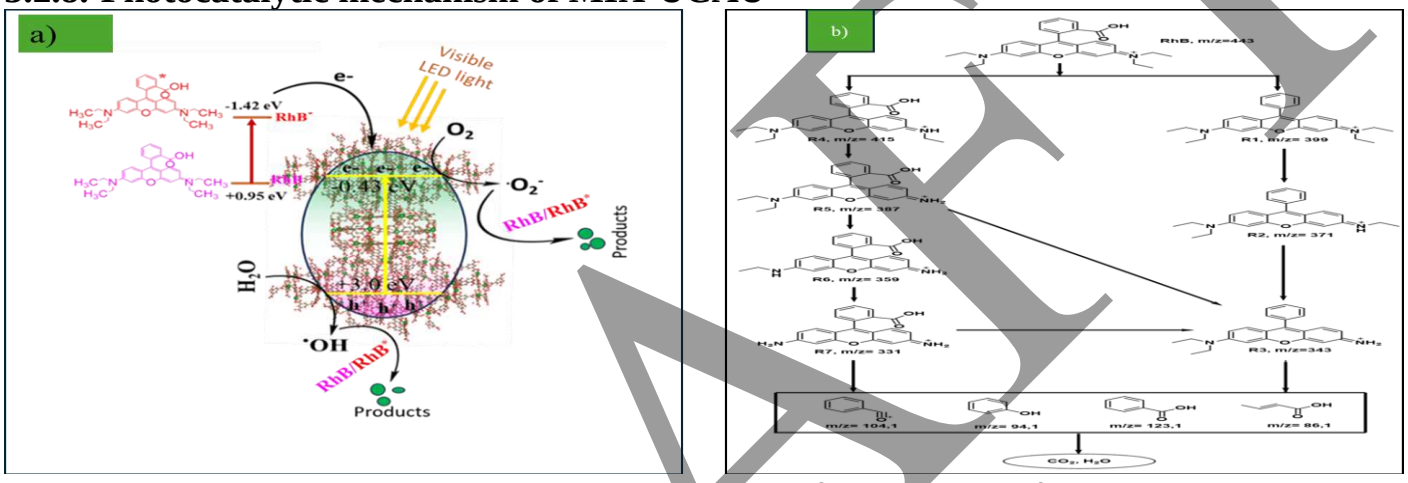


Figure 3.13: (a) Proposed Photocatalytic Mechanism of MIX-UCAU for RhB Degradation, (b) Proposed Degradation Pathway of RhB on MIX-UCAU Catalyst

The CAU-17 and UU-200 materials exhibit RhB degradation efficiency of 98%, comparable to that of the BiBDC material, as described in section 3.1. However, they achieve this efficiency within a reduced degradation time of only 120 minutes and with a lower material dosage (20 mg compared to 30 mg for BiBDC). The enhanced photocatalytic activity of CAU-17 and UU-200, compared to BiBDC, can be explained by an increase number of charge transfer states from the ligand to the metal center. To further enhance the degradation efficiency of RhB, a Metal-Organic Framework (MOF) comp osite material, MIX-UCAU, was synthesized by integrating UU-200 and CAU-17. MIX-UCAU exhibits a higher crystallinity and better light absorption capability compared to the individual UU-200 and CAU-17 materials. Bi-MOF-based materials, including BiBDC, CAU-17, UU-200, and MIX-UCAU, all show photocatalytic activity for the degradation of organic pollutants. However, the large bandgap energy of Bi-MOFs materials limits their application potential. To address this limitation and enhance photocatalytic properties, composite materials such as CAU-17/BiOCl and BiOCl/BHP have been developed. These composites improve bandgap energy and broaden the applicability of Bi-MOF-based photocatalysts.

Figure 3.13 indicates that RhB undergoes photocatalytic degradation into various intermediate products through processes like carboxylation, alkylation, amination, and ring cleavage, ultimately mineralizing into smaller molecules. In the first reaction pathway, RhB (m/z = 443) is carboxylated to form R1 (m/z = 399), which subsequently undergoes dealkylated to form R2 (m/z = 371) and R3 (m/z = 343). In the second pathway, RhB undergoes N-dealkylation, resulting the formation of intermediates R4 (m/z = 415), R5 (m/z = 387), R6 (m/z

DRAFT

= 359), and R7 (m/z = 331). These intermediates are further broken down into smaller by-products through ring cleavage, such as benzylidyneoxonium (m/z = 104), phenol (m/z = 94), benzoic acid (m/z = 123), and butenoic acid (m/z = 86). These smaller molecules are eventually degrade into final products like CO_2 and H_2O.

3.3. Synthesis of CAU-17/BiOCl composite and its application as a photocatalyst for RhB and TC degradation

3.3.1. Results of Synthesis of CAU-17/BiOCl Composite System

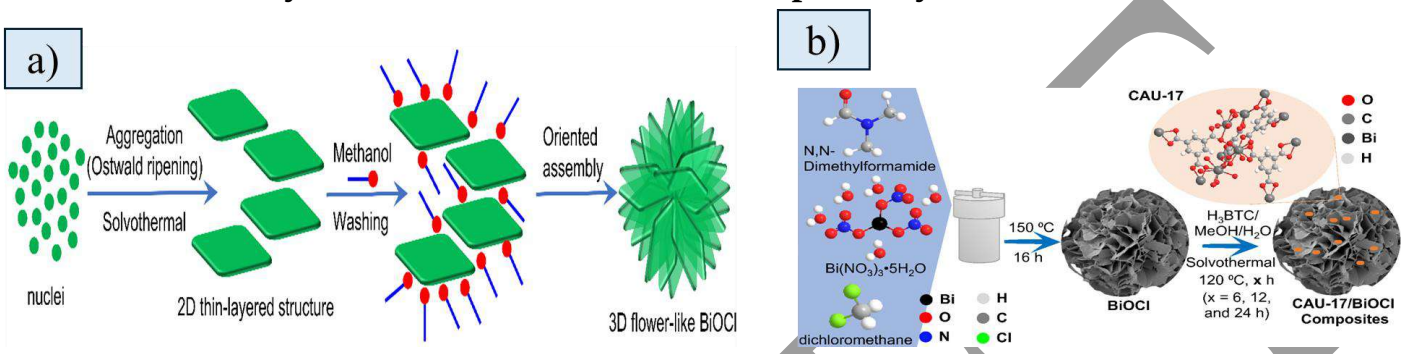


Figure 3.14: (a) Proposed Mechanism for the Formation of 3D Flower-Like Structures of BiOCl, (b) Schematic of the Formation of CAU-17/BiOCl Composite.

The CAU-17/BiOCl composite system is synthesized by developing thin layers of CAU-17 on the surface of flower-like BiOCl nanoplates using a solvothermal method, as described in Figures 3.14. The successful synthesis of the CAU-17/BiOCl composite results in the in-situ formation of CAU-17 on BiOCl crystals.

3.3.2. Results of crystal structure and thermal properties analysis of CAU-17/BiOCl material

The XRD pattern identifying the crystal structures of CAU-17, BiOCl, and CAU-17/BiOCl is shown in Figure 3.15. The XRD pattern of CAU-17 exhibits diffraction peaks corresponding to the characteristic peaks of CAU-17 (CCDC 1426169), which have been reported previously. The diffraction peaks of BiOCl are consistent with its tetragonal form (JCPDS 06-0249). In the CAU-17/BiOCl heterojunction system, the peaks corresponding to CAU-17 are detected alongside those of BiOCl; however, the intensity of the (001) plane of BiOCl significantly decreases. This suggests that CAU-17 forms on the [001] faces of BiOCl crystals. Additionally, extending the solvothermal reaction time leads to an increase in the crystallinity ratio of CAU-17, indicating that the phase transition from BiOCl to CAU-17 can be controlled by adjusting the reaction time.

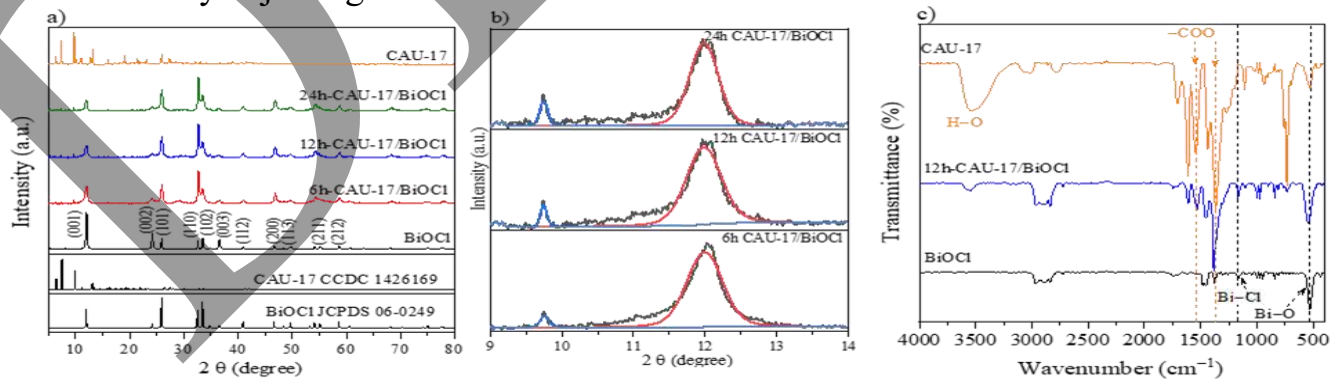


Figure 3.15: (a-b) XRD Pattern of the xh-CAU-17/BiOCl Material, (c) FT-IR Spectrum of CAU-17, BiOCl, and 12h-CAU-17/BiOCl materials

To determine the chemical bonds of the BiOCl, CAU-17/BiOCl, and CAU-17 materials, FT-IR spectroscopy was performed (Figure 3.15 c). The absorption peak at 525 cm^{-1} corresponds to the stretching vibration of Bi−O, the broad peak at 3530 cm^{-1} is attributed to the O−H vibration of H_2O. A weak peak at 1377 cm^{-1} corresponds to the C−N stretching

DRAFT

vibration in BiOCl, which may be due to a small amount of DMF adsorbed on the surface of BiOCl. In addition, the peak around 1164 cm^{-1} is attributed to the Bi−Cl vibration in BiOCl. A slight shift in the characteristic wavenumbers of CAU-17 in the 12h-CAU-17/BiOCl composite material compared to CAU-17 confirms the interaction between BiOCl and CAU-17.

The XPS spectra of BiOCl, CAU-17, and 12h-CAU-17/BiOCl were analyzed to identify the chemical composition and oxidation states of the elements. As shown in Figure 3.1 (a), the XPS spectrum of BiOCl shows the presence of Bi, O, and Cl in BiOCl. For CAU-17, the detected elements include Bi, C, and O. The 12h-CAU-17/BiOCl composite contains Bi, C, O, and Cl, in agreement with the EDS measurements shown in Figure 3.16 (b-e). These XPS results confirm that the formation of CAU-17/BiOCl heterojunction on the flower-like BiOCl surface has been successfully synthesized. The C 1s spectrum is deconvoluted into three main peaks, confirming the presence of CAU-17 in the composite. The Cl 2p spectrum shows a shift in the binding energy peaks when CAU-17 is formed on the BiOCl surface, indicating a change in the electron density around the Cl atoms. For Bi 4f, the characteristic peaks show a binding energy shift of more than 0.3 eV, suggesting the formation of O−Bi bonds between BiOCl and CAU-17. The O 1s spectrum is deconvoluted into four peaks, with a significant shift in the Bi−O binding, indicating a substantial charge transfer at the Bi−O chemical interface. These binding energy shifts indicate a strong interaction between CAU-17 and BiOCl, which enhances photocatalytic activity by promoting effective electron-hole separation within the heterojunction system.

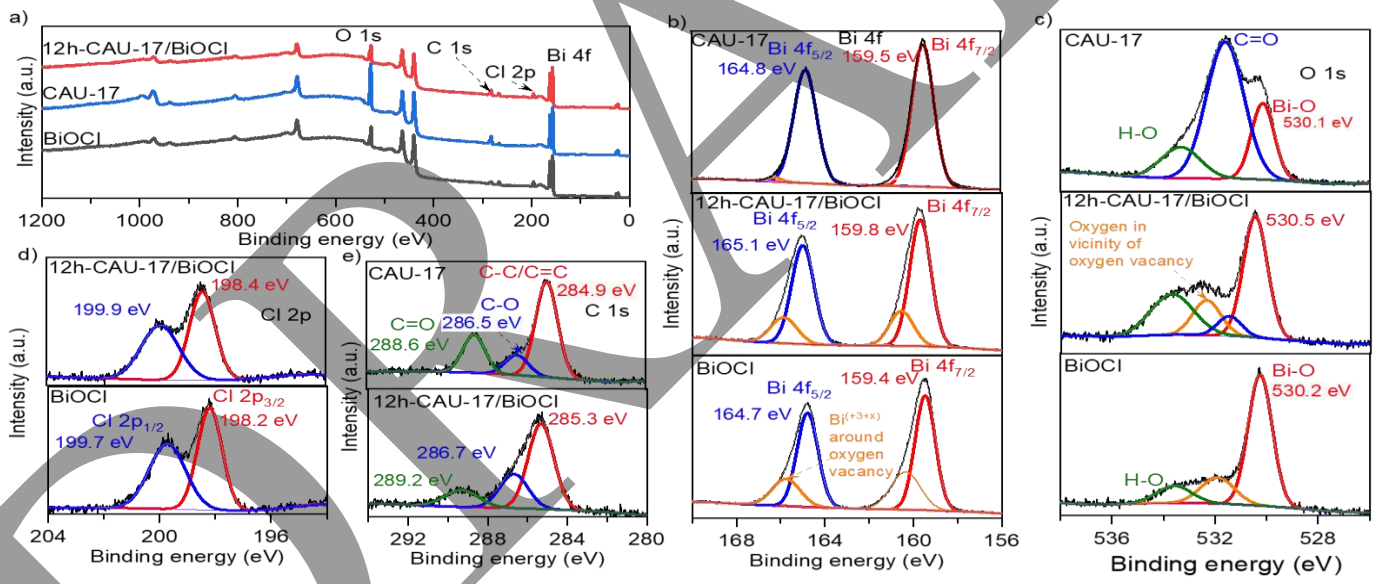


Figure 3.17: (a) XPS spectrum of BiOCl, CAU-17, and 12h-CAU-17/BiOCl; (b-e) XPS Spectra of (b) Bi 4f, (c) O 1s, (d) Cl 2p, (e) C 1s.

3.3.3. Results of the morphological characterization of the CAU-17/BiOCl material.

The morphology of the CAU-17/BiOCl composites with different solvothermal reaction times was observed through SEM images (Figure 3.17). The SEM images show that the CAU-17/BiOCl composite consists of thin layers of CAU-17 embedded within the gaps of BiOCl crystal, while the flower-like structure of BiOCl remains intact. The CAU-17 material exhibits a cylindrical structure, with stacked layers that increases the surface area, thus facilitating the absorption of reactants. EDS analysis reveals an even distributed of carbon across the surface of BiOCl, confirming the uniform growth of the CAU-17 layers. TEM images ((Figure 3.18) further corroborate that BiOCl maintains a smooth surface, while CAU-17 features cylindrical structures. After 12 hours of synthesis, the surface of BiOCl becomes rougher due to the growth

DRAFT

of the CAU-17 layers. This observation supports the formation of a heterojunction surface between the two components, which may enhance photocatalytic activity by improving charge separation.

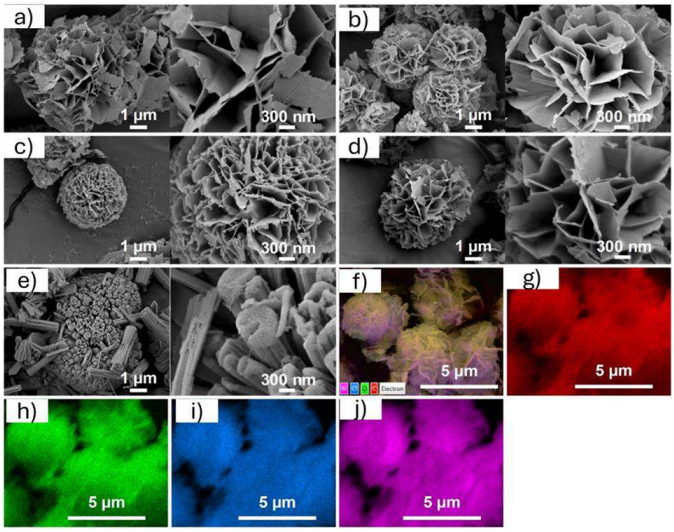


Figure 3.17: SEM images and elemental mapping of the materials: (a) BiOCl, (b) 6h-CAU-17/BiOCl, (c) 12h-CAU-17/BiOCl, (d) 24h-CAU-17/BiOCl, (e) CAU-17, (f) SEM-EDS image of 12h-CAU-17/BiOCl, and (g-j) elemental distribution maps of 12h-BiOCl/BHP for C (g), O (h), Cl (i), and Bi (j).

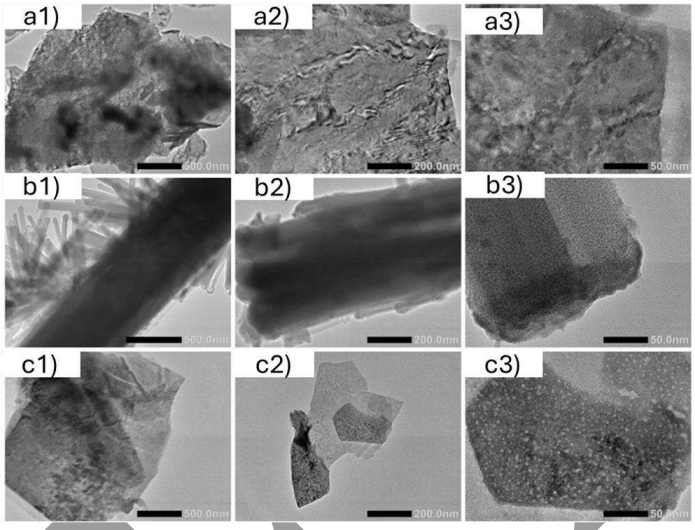


Figure 3.18: TEM images of BiOCl (a1–a3), CAU-17 (b1–b3), and 12h-CAU-17/BiOCl (c1–c3) captured at different scale bars.

3.3.4. Optical and electrochemical properties of CAU-17/BiOCl material

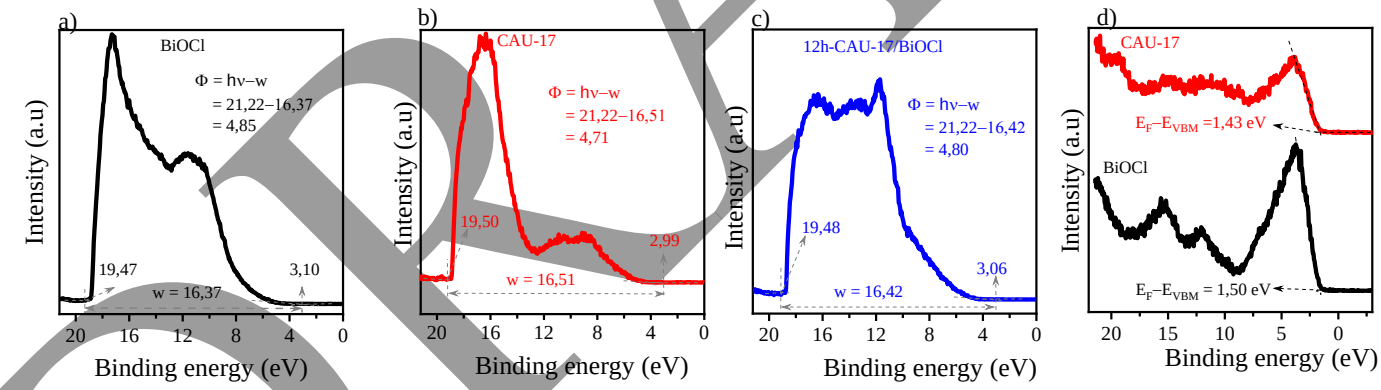


Figure 3.19: (a) UPS pattern of BiOCl, (b) CAU-17 and 12h-CAU-17/BiOCl, (c) XPS-VB pattern of BiOCl and CAU-17

The electron energy of the atoms on the surface of the material was determined using the ultraviolet photoelectron spectroscopy (UPS) (Figure 3.19 (a-b)). The work function (Φ) values for BiOCl, CAU-17, and 12h-CAU-17/BiOCl were determined to be 4.85, 4.71, and 4.80 eV (Φ relative to vacuum), respectively. The electron energy in the valence band of the materials was determined using the VB-XPS (Figure 3.19 (c)). The energy difference between the Fermi level and the valence band maximum ($E_F - E_{VBM}$) for BiOCl and CAU-17 were determined to be +1.50 eV and +1.43 eV, respectively.

The UV-Vis DRS results, employed to assess the light absorption capability of the material, are shown in Figure 3.20 (a). The E_g values of the semiconductors were determined by plotting a Tauc plot, as shown in Figure 3.20 (b). The CAU-17/BiOCl heterojunction composites, formed by depositing the CAU-17 layer on the surface of flower-like BiOCl through the solvothermal method over different reaction times (6h, 12h, and 24h), exhibit a

DRAFT

bandgap energy of approximately 2.84–2.95 eV. These bandgap energy is lower compared to that of the individual CAU-17 and BiOCl materials, indicating that the interaction between CAU-17 and BiOCl alters the electronic structure, resulting in a significant reduction in the bandgap energy of the heterojunction system. The Mott-Schottky plot (Figure 3.20 (c)). indicates that both CAU-17 and BiOCl are n-type semiconductors. This electronic compatibility enables the construction of the CAU-17/BiOCl heterojunction, which promotes the efficient separation of electron-hole pairs. PL analysis Figure 3.20 (d) indicates a decrease in PL intensity when CAU-17 is formed on the surface of BiOCl, indicating improved separation of the electron-hole pairs. EIS results further confirm efficient electron movement within the CAU-17/BiOCl heterojunction system, contributing to enhanced photocatalytic performance.

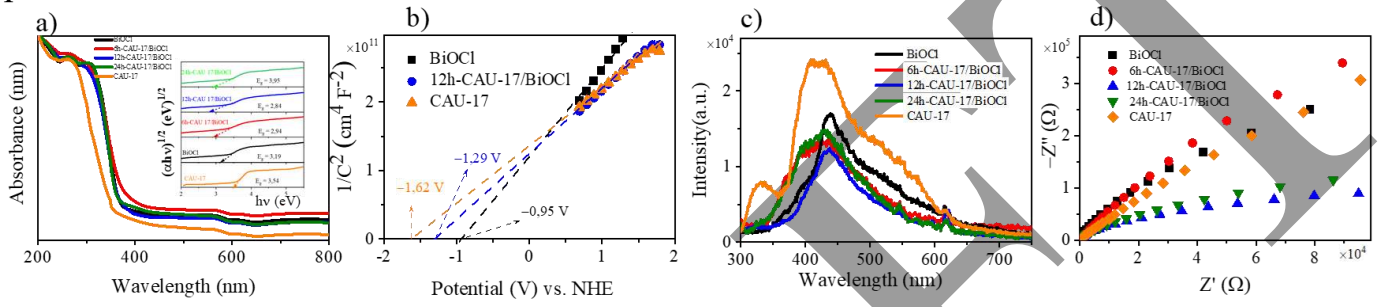


Figure 3.20: (a) UV-Vis Diffuse Reflectance Spectrum; (b) Mott-Schottky Analysis; (c) Photoluminescence spectrum; (d) Nyquist Plot.

3.3.5. Photocatalytic Degradation of RhB by CAU-17/BiOCl Material

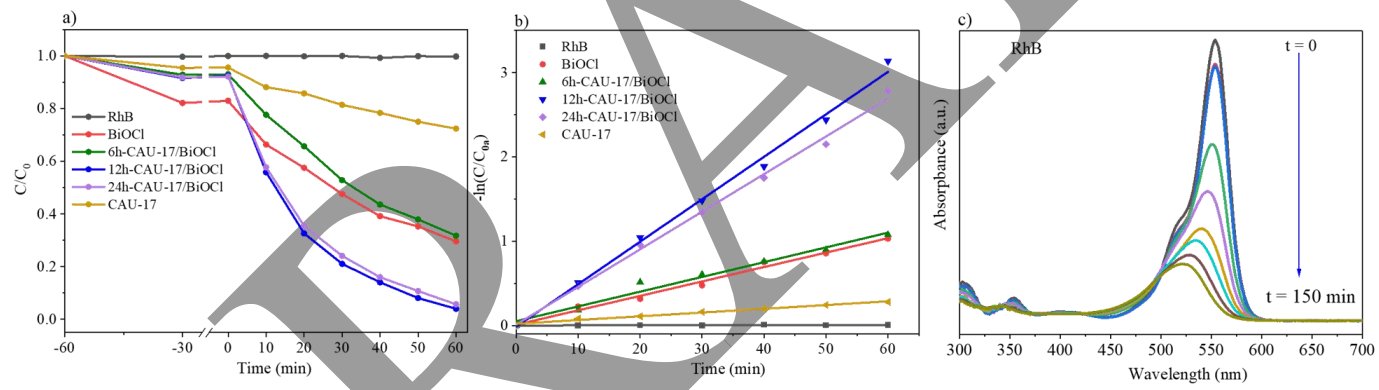


Figure 3.21: (a) Photocatalytic activity; (b) kinetic equation for RhB degradation; (c) UV-vis absorption spectra of RhB solution during photocatalytic reaction using 12h-CAU-17/BiOCl.

The degradation reaction of RhB occurs in two main stages: adsorption and photodegradation, as shown in Figure 3.21. To accurately evaluate the photocatalytic degradation efficiency, RhB must first reach equilibrium adsorption before irradiation. The adsorption efficiency of RhB follows the order: BiOCl > CAU-17/BiOCl > CAU-17, with BiOCl exhibiting a negatively charged surface that adsorbs cationic dyes like RhB more effectively. After 1 hour of catalysis, BiOCl and CAU-17 achieve RhB degradation efficiencies of 70.4% and 41.2%, respectively, while the optimal composite CAU-17/BiOCl achieves 96% degradation of RhB. A first-order kinetic model was used to estimate the reaction rate constant (k), resulting in the following order: 12h-CAU-17/BiOCl > 24h-CAU-17/BiOCl > 6h-CAU-17/BiOCl > BiOCl > CAU-17. The optimal ratio of CAU-17 improves photocatalytic performance by balancing electron transfer capabilities and the formation of electron-hole pairs. The decrease and shift of the UV-Vis absorption peak of RhB towards shorter wavelengths indicate that the reduction in RhB concentration occurs mainly through the photocatalytic mechanism, rather than adsorption, leading to the degradation of RhB.

DRAFT

The reuse results for the12h-CAU-17/BiOCl photocatalyst (Figure 3.22) showed that the RhB degradation efficiency decreased from 96% to 90% after the fourth use. This reduction in photocatalytic activity after multiple uses is attributed to the adsorption of RhB molecules or intermediate compounds on the catalyst surface, which reduces the availability of active sites for the catalytic process.

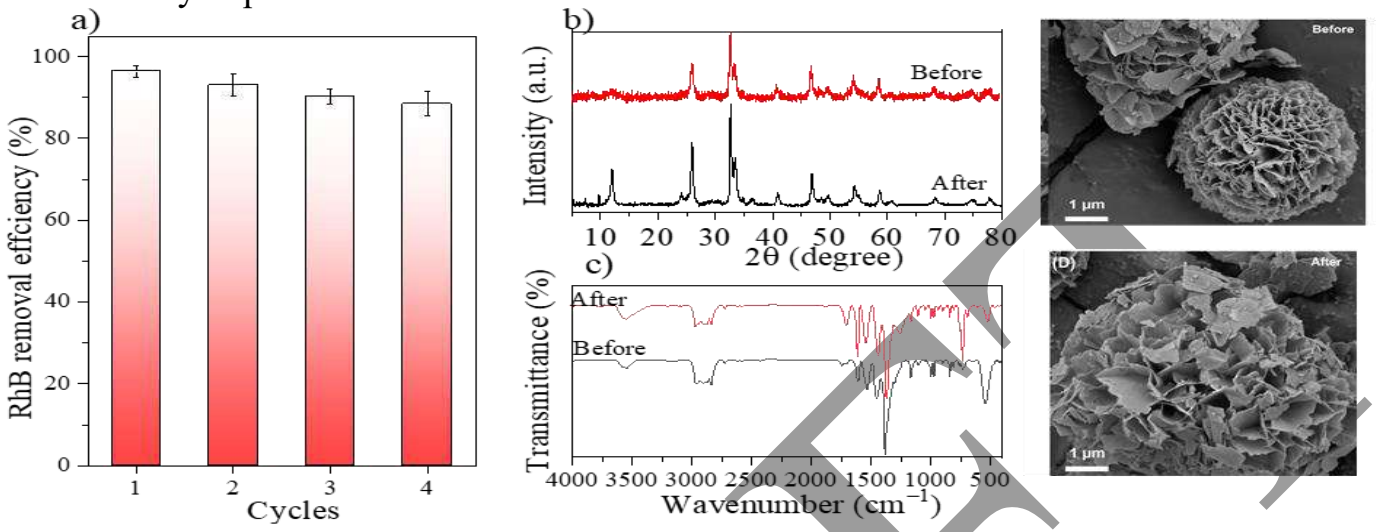
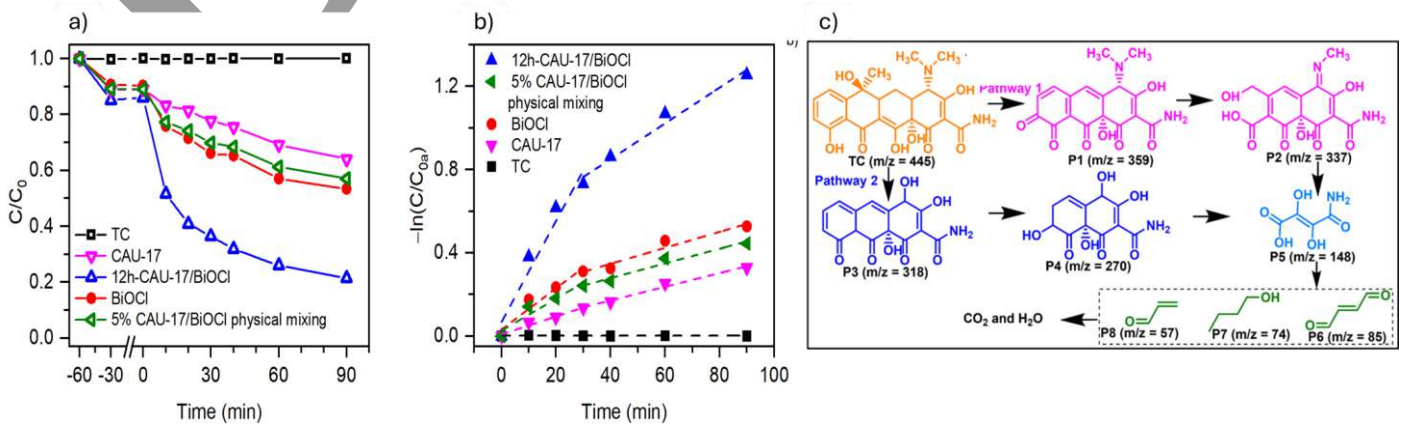


Figure 3.22: Plot of RhB removal efficiently versus the number of 12h-CAU-17/BiOCl catalyst reuses

3.3.6. Photodegradation of TC by CAU-17/BiOCl Material

The photocatalytic performance of 12h-CAU-17/BiOCl was evaluated for the degradation of TC (Figure 3.23 (a-b)). After 90 minutes of irradiation, the composite achieved a TC degradation efficiency of 78.4%, outperforming CAU-17 (35.9%) and BiOCl (46.6%). A physical mixture of 5% CAU-17 and 95% BiOCl exhibited significantly lower efficiency compared to the 12h-CAU-17/BiOCl composite, underscoring the importance of a heterojunction between CAU-17 and BiOCl in enhancing photocatalytic performance. The TC degradation process occurs in two stages: an initial stage involving rapid reactions such as dehydration, demethylation, oxidation, and deamination, followed by a later stage dominated by ring-opening reactions of intermediate compounds with lower molecular weights than the original TC. The 12h-CAU-17/BiOCl composite demonstrated the highest degradation rate constant of 24.3 × 10^{-3} min^{-1}, which is 3.2 times higher than that of CAU-17 and 2.4 times higher than BiOCl. These findings highlight the significantly superior photocatalytic efficiency of the composite compared to the individual materials. The enhanced degradation rate constant indicates that the heterojunction between CAU-17 and BiOCl promotes efficient electron transfer and electron-hole pair separation, thereby improving photocatalytic performance. The intermediate products formed during TC degradation were identified using LC-MS, and the proposed degradation pathways are illustrated in Figure 3.23 (c).



DRAFT

Figure 3.23: (a) Photocatalytic Activity for TC Degradation, (b) Kinetic Equation for TC Degradation Using CAU-17/BiOCl Photocatalyst, (c) Proposed TC Degradation Pathway Using the 12h-CAU-17/BiOCl Catalyst.

3.3.7. Photocatalytic Mechanism of CAU-17/BiOCl

The results presented in Figure 3.24 show that $\bullet O_2^-$, e^-, and h^+ are the main species responsible for the degradation of RhB and TC when exposed to visible light. Based on experimental findings, the thesis proposes the photocatalytic mechanism of CAU-17/BiOCl for degrading organic pollutants, as illustrated in Figure 3.24. Electrons in CAU-17 are transferred to BiOCl due to the formation of an internal electric field (IEF) at the interface between the two materials. This IEF induces the formation of electron-deficient and electron-rich layers near the surfaces of CAU-17 and BiOCl, respectively. Under LED light irradiation, the IEF drives the migration of charge carriers from BiOCl to CAU-17, effectively inhibiting the recombination of the electron-hole pairs. The CAU-17/BiOCl heterojunction facilitates both reduction and oxidation reactions, enabling efficient degradation of RhB and TC. Based on the energy band structure of CAU-17/BiOCl, electrons from BiOCl migrate to the surface of CAU-17, while the strongly oxidizing holes remain in BiOCl. Electrons and holes participate in reactions with RhB or TC, ultimately leading to their breakdown into CO_2 and H_2O.

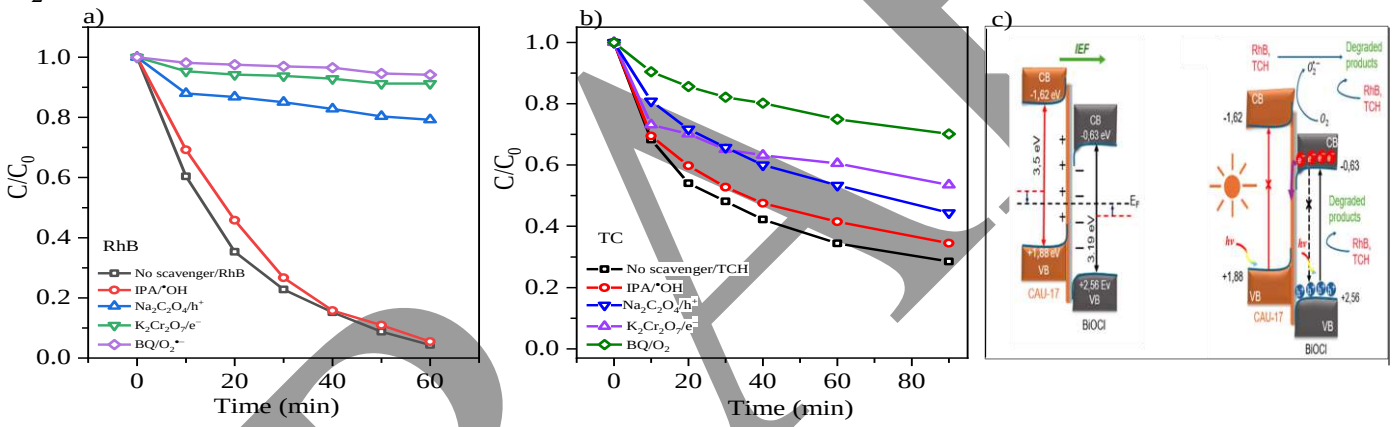


Figure 3.24: Photocatalytic Activity of 12h-CAU-17/BiOCl in the Presence of scavengers for the degradation of (a) RhB and (b) TC, c) Schematic illustration of the CAU-17/BiOCl heterojunction and Proposed photocatalytic mechanism of CAU-17/BiOCl for RhB and TC degradation

3.4. Synthesis of BiOCl/BHP composite and its application as a photocatalyst for the degradation of RhB and SMX

3.4.1. Synthesis results of the BiOCl/BHP material from CAU-17

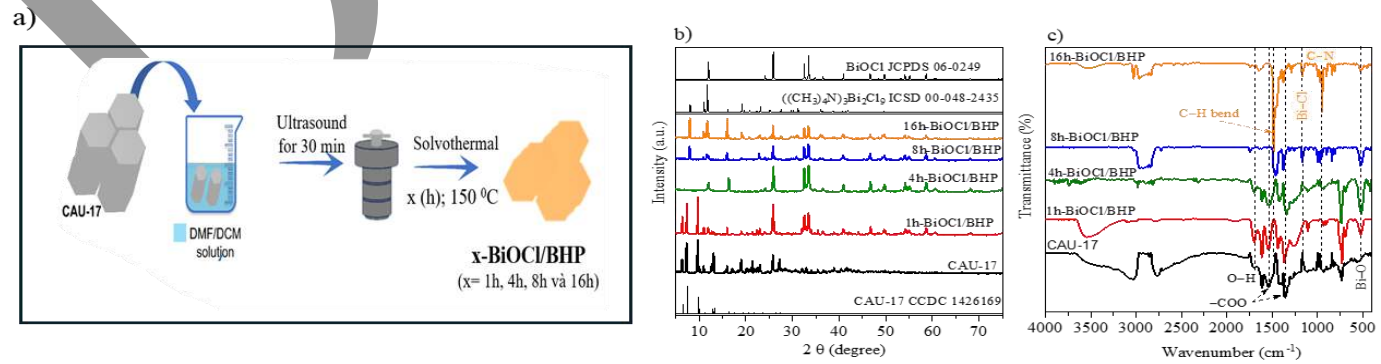


Figure 3.25: (a) Schematic Illustration of the Formation of BiOCl/BHP Material from CAU-17, (b) XRD Diffraction Pattern; (c) FT-IR Spectrum of BiOCl/BHP

DRAFT

The BiOCl/BHP material was syntheisized via a solvothermal reaction involving CAU-17 in a solvent system of DMF ($(CH_3)_2NCHO$) and DCM (CH_2Cl_2) at a temperature of 155°C. The duration of the solvothermal process was varied, with reaction times of 1, 4, 8, and 16 hours, as described in figure 3.25 (a).

The XRD pattern shown in Figure 3.25 (b) indicates that, with an increase in solvothermal reaction time, the characteristic peaks of CAU-17 progressively diminish, while peaks corresponding to BiOCl (JCPDS 06–0249) and BHP (ICSD 00-048-2435 for $((CH_3)_4N)_3Bi_2Cl_9$) become more prominent. This outcome demonstrates the gradual development of BiOCl and BHP crystals on the surface of CAU-17. The FT-IR analysis (Figure 3.25 (c)) confirms the presence of Bi–O, Bi–Cl, C–H, and C–N bonds within the BiOCl/BHP material, highlighting the role of solvothermal reaction time in the formation and evolution of these crystal structures.

XPS analysis (analysis (Figure 3.26) further validates the synthesis of the BiOCl/BHP composite by confirming the presence of Bi, C, O, N, and Cl elements. The high-resolution XPS spectrum of N 1s reveals N–C and N–C bonds in BHP, while slight shifts in the binding energy of the Bi 4f peaks, suggesting the formation of Bi–Cl bonds and a reduction in the oxidation state of Bi, due to oxygen deficiency. Furthermore, the C 1s and O 1s spectra indicate the presence of C–N, C–N, Bi–O, and O–H bonds. The observed shifts in binding energy for the Bi 4f, Cl 2p, and O 1s spectra demonstrate the electronic interaction between BiOCl and BHP, substantiating the formation of the BiOCl/BHP heterostructure.

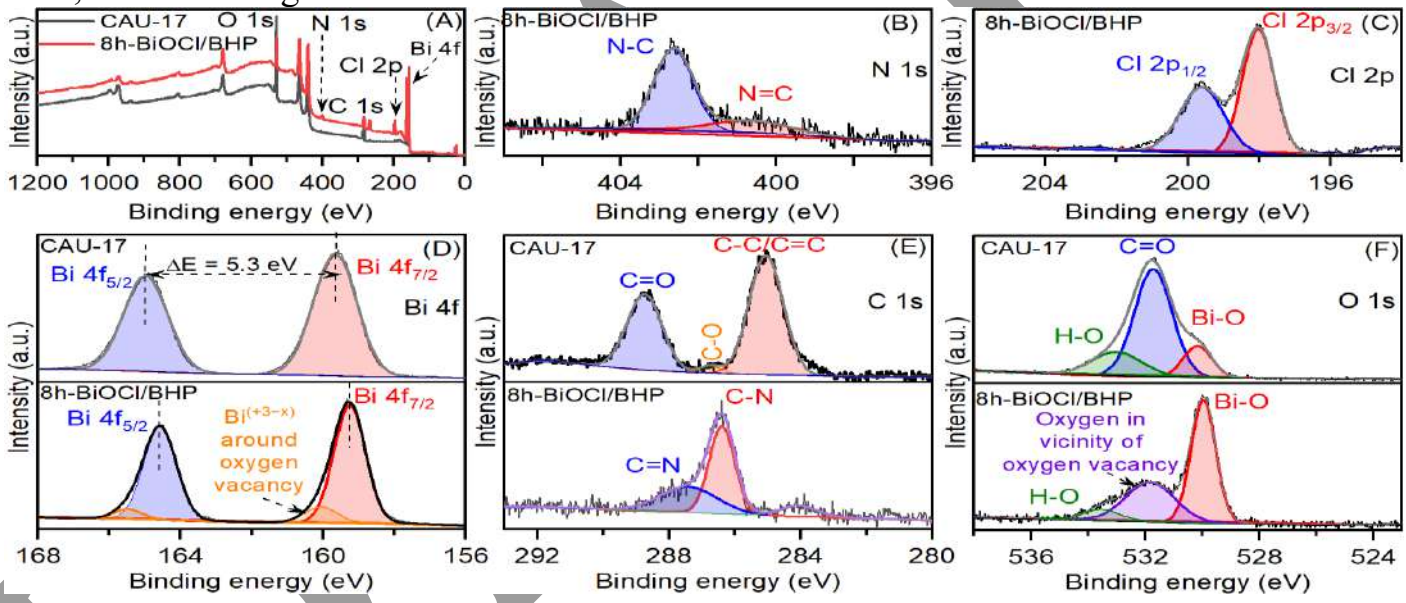


Figure 3.26: (a) XPS Spectrum of CAU-17 and 8h-BiOCl/BHP; (b-f) XPS Spectra of (b) N 1s, (c) Cl 2p, (d) Bi 4f, (e) C 1s, and (f) O 1s.

3.4.2. Results of Surface Morphology Characterization of BiOCl/BHP Material

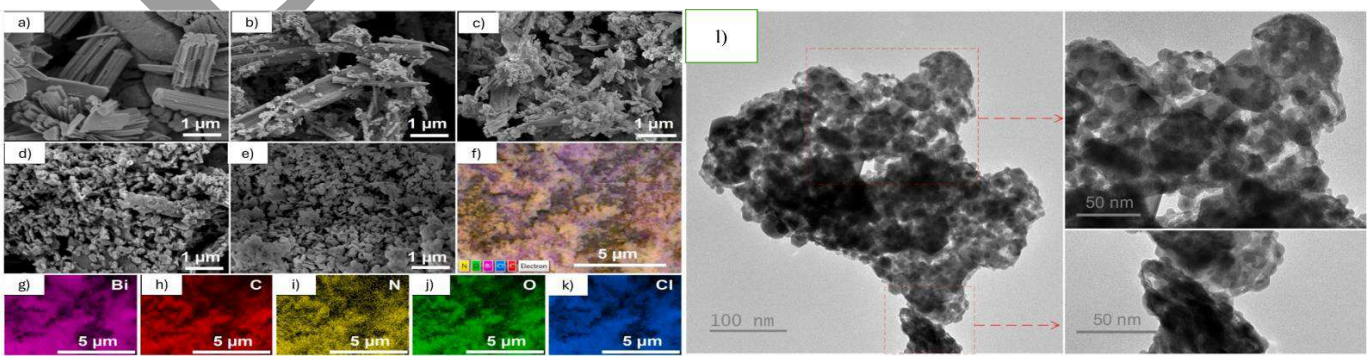


Figure 3.27: SEM Images of (a) CAU-17, (b) 1h-BiOCl/BHP, (c) 4h-BiOCl/BHP, (d) 8h-BiOCl/BHP, (e) 16h-BiOCl/BHP, (f) SEM-EDS Image, (g-k) Elemental Distribution Maps in the 8h-BiOCl/BHP, (l) TEM Image of the 8h-BiOCl/BHP

The SEM images in Figure 3.27 show that the CAU-17 material exhibits a rod-like structure with dimensions ranging from 0.9 to 2.3 µm. Following 1 hour of solvothermal treatment in a DMF/DCM solvent system, the formation of BiOCl flakes alongside the rod-like structure begins to emerge. As the reaction time is extended to 8 hours and 16 hours results the BiOCl/BHP composites develop a distinct nano-sheet morphology, characterized by predominantly circular and oval shapes with crystal diameters ranging from 50 to 200 nm. EDS and TEM results confirm the uniform distribution of Bi, C, O, Cl, and N elements within the material. Moreover, the TEM images highlight the formation of a well-defined junction between BiOCl and BHP. This heterojunction structure is instrumental in enhancing charge separation and transfer, thereby contributing to improved photocatalytic efficiency in the BiOCl/BHP composite system.

3.4.4 Results of optical and electrochemical properties of the BiOCl/BHP material

The UV-vis DRS spectra of BiOCl/BHP (Figure 3.28 (a, b)) indicate a shift in the light absorption around 426 nm, which enhances light absorption and photocatalytic efficiency of materials. As the solvothermal reaction time for CAU-17 increases, the E_g values of the BiOCl/BHP material decreases significantly, from 3.71 eV to 2.69 eV. The photoluminescence (PL) spectra and Nyquist plots shown in Figure 3.28 (c, d) reveal enhanced charge separation and mobility in BiOCl/BHP, especially in the 8h-BiOCl/BHP material, which exhibits superior photocatalytic efficiency. Mott-Schottky measurements presented confirm that both BiOCl and BHP exhibit n-type semiconductor properties.

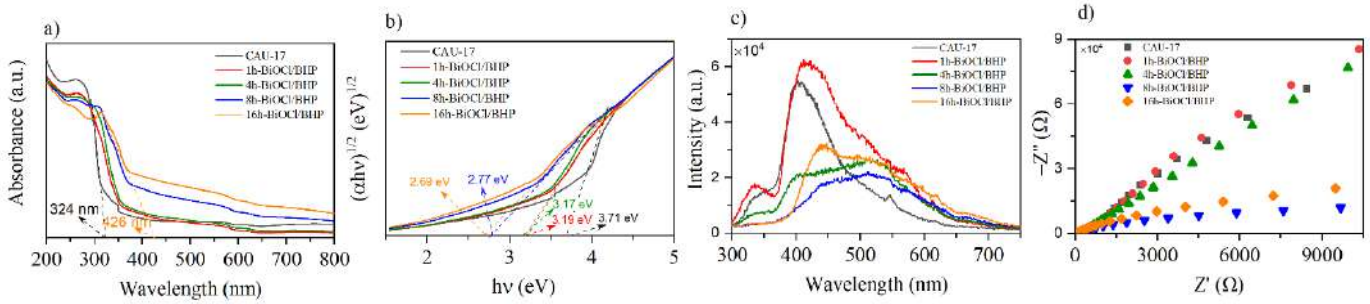


Figure 3.28: (a) UV-Vis Diffuse reflectance spectrum (DRS); (b) Band gap energy of the synthesized samples; (c) Photoluminescence (PL) spectrum of the synthesized samples; (d) Nyquist plot of CAU-17 and xh-BiOCl/BHP.

3.4.5. Photocatalytic degradation of RhB and SMX by BiOCl/BHP material

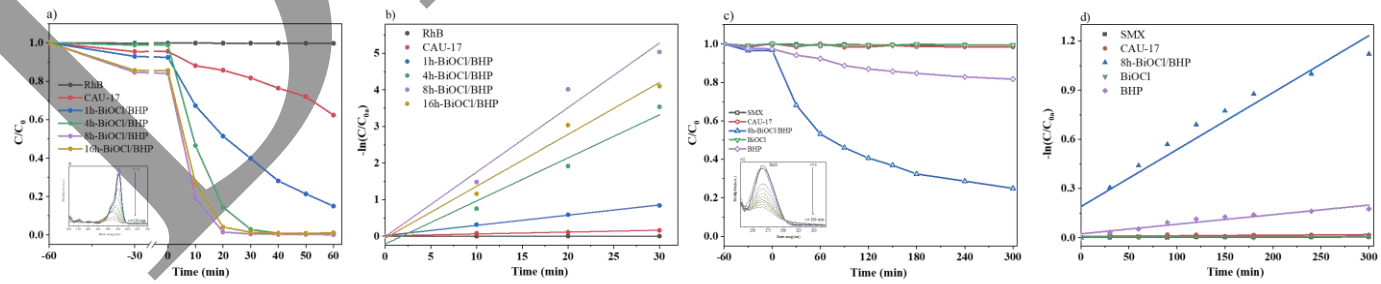


Figure 3.29: (a) Photocatalytic Activity RhB; (b) Kinetic Equation for RhB (c) Photocatalytic activity SMX; (d) Kinetic equation of photocatalysis for SMX degradation using BiOCl/BHP Catalyst.

The photocatalytic performance results for RhB degradation (Figure 3.29) demonstrate that the xh-BiOCl/BHP material exhibits superior efficiency compared to CAU-17. Specifically, the 8h-BiOCl/BHP material achieved over 99.4% degradation of RhB after 30

minutes of light exposure, and achieved 99.8% degradation after 60 minutes of irradiation. Its apparent rate constant, 176.45 × 10^{-3} min^{-1}, is significantly higher than that of the individual materials. The lower efficiency of 1h-BiOCl/BHP and 4h-BiOCl/BHP materials is due to their reduced BHP content, which limits the ability of material to separate the electron-hole effectively. Furthermore, the 16h-BiOCl/BHP material, with an excessive BHP content, showed reduced performance because of the rapid recombination of photogenerated electrons and holes. PL and EIS analyses confirmed that the surface interaction between BiOCl and BHP enhances charge separation and transfer, improving photocatalytic efficiency.

The photocatalytic degradation efficiency of SMX over CAU-17, 8h-BiOCl/BHP, BiOCl, and BHP was 1.5%, 75.1%, 0.6%, and 18.3%, respectively. The 8h-BiOCl/BHP material demonstrated the highest catalytic activity, with a rate constant (k = 3.48 × 10^{-3} min^{-1}), which is 6 times higher than that of pure BHP. HPLC analysis revealed that the 8h-BiOCl/BHP material achieved nearly complete SMX degradation, with 93.9% degradation after 300 minutes of irradiation.

As shown in Figure 3.30 (a-d), after four cycles of use, the RhB degradation efficiency of the 8h-BiOCl/BHP material decreased from 99.8% to 86.5%, indicating some loss of activity due to surface adsorption of intermediates or degradation products, which may block active sites.

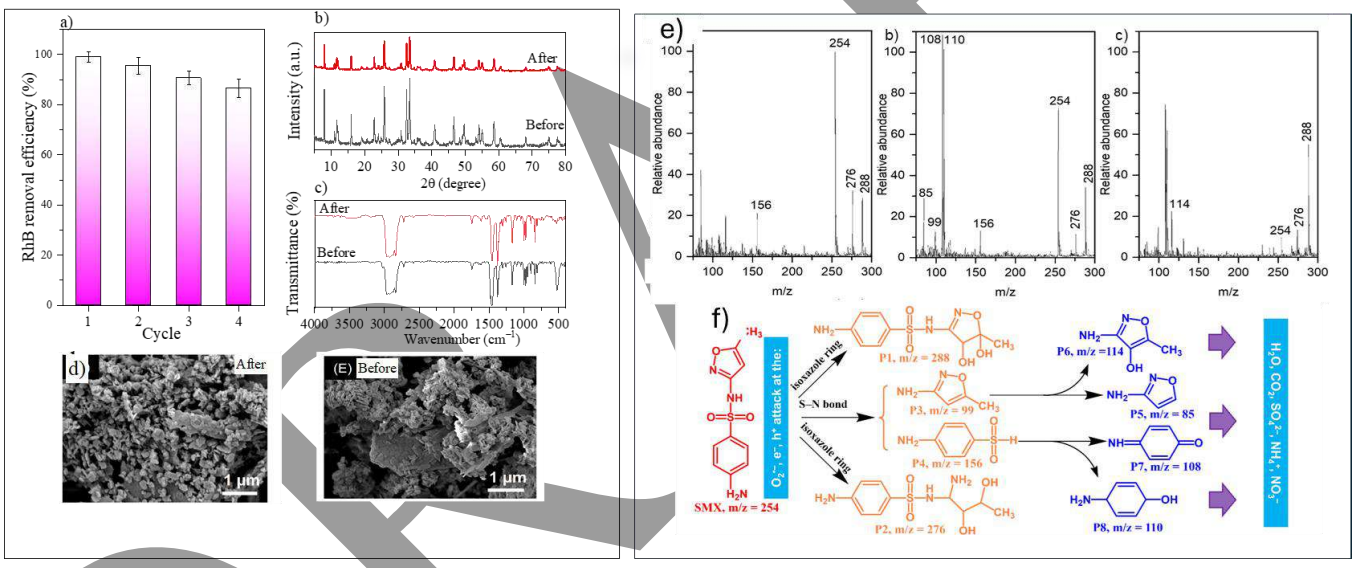


Figure 3.30: (a-d) Photocatalytic Efficiency of 8h-BiOCl/BHP After Reuse for RhB Degradation; (e) LC-MS spectrum of possible SMX intermediate products at different reaction times, (f) Proposed degradation pathway of SMX using 8h-BiOCl catalyst

3.4.6. Photocatalytic Mechanism

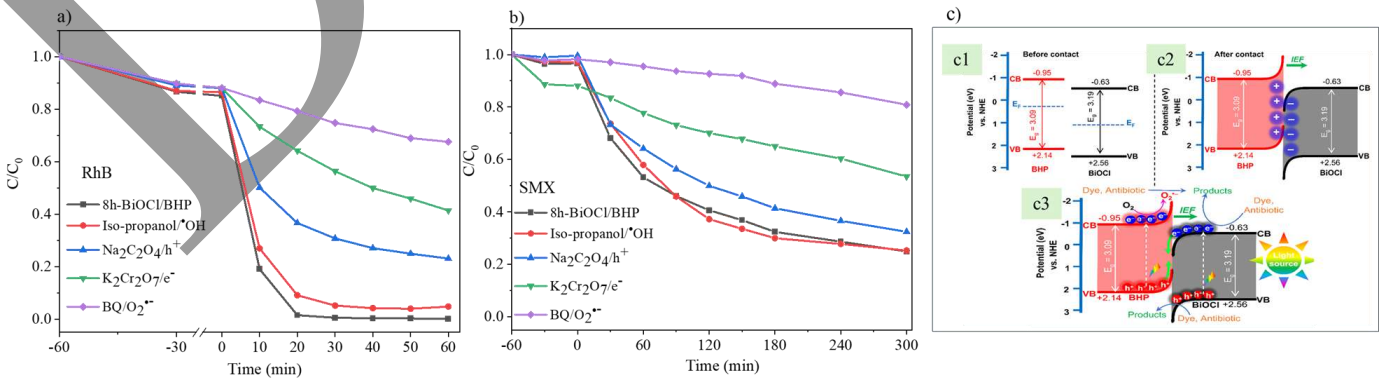


Figure 3.31 (a-b) Effect of radical scavengers on the degradation process of (a) RhB and (b) SMX using 8h-BiOCl/BHP material. (c) Illustration of the energy band structure of the BiOCl/BHP heterojunction

DRAFT

The photocatalytic activity results of 8h-BiOCl/BHP with radical scavengers for the degradation of RhB and SMX are shown in Figure 3.31. The degradation efficiency of RhB significantly decreases when BQ is introduced as a scavenger, followed by $K_2Cr_2O_7$ and $Na_2C_2O_4$. These results indicate that $\bullet O_2^-$ and e^- play a crucial role in the photocatalytic degradation of RhB and SMX, while h^+ plays a secondary role in this process. The study proposes an electron transfer mechanism in the BiOCl/BHP heterojunction based on the S-Scheme model. In this mechanism, electrons transfer from BHP to BiOCl, while holes transfer in the opposite direction, resulting in the formation of an internal electric field (IEF). This IEF effectively separates the electron-hole pairs, thereby minimizing recombination. Additionally, the formation of interaction between BiOCl and BHP, formed through the optimized solvothermal reaction of CAU-17, enhances the efficiency of charge separation and establism effective charge transport channels. These channels enable electrons and holes to rapidly migrate to the catalyst surface, where they participate in photocatalytic reactions, such as the degradation of organic pollutants. The strong interfacial interaction within the heterojunction significantly improves photocatalytic efficiency, as evidenced by the enhanced degradation performance for RhB and SMX.

We successfully synthesized BiOCl/BHP S-scheme heterostructure photocatalysts derived from CAU-17 using an in situ solvothermal method under mild conditions. The photocatalytic efficiency of these materials was assessed by measuring the degradation rates of RhB and SMX. The BiOCl/BHP composites exhibited a high responsiveness to LED light and an enhanced charge migration pathway of photoexcited charges, attributed to the formation of the BiOCl/BHP S-scheme heter- ojunction. Remarkably, the 8h-BiOCl/BHP composite demonstrated su- perior removal efficiencies, achieving 99.8% for RhB within 60 min and 75.1% for SMX within 300 min. Active species capture experiments verified $\bullet O_2^-$, e^-, and h^+ as the primary active species involved in the photocatalysis process. Based on these results, we proposed a plausible photocatalytic reaction mechanism that relies on the S-scheme hetero-junction formed by the BiOCl/BHP composite. This study introduces an innovative approach to the development of highly efficient S-scheme heterostructure photocatalysts derived from MOFs, with a particular focus on eliminating organic pollutants.

DRAFT

CONCLUSION AND RECOMMENDATIONS

CONCLUSION

In this dissertation, various Bi-MOF materials and their composite are successfully synthesized using a solvothermal method, such as BiBDC, CAU-17, UU-200, MIX-UCAU composite, CAU-17/BiOCl composite, and BiOCl/BHP composite. The synthesized materials were comprehensively characterized in terms of crystal structure, thermal properties, surface morphology, optical properties, and electrochemical characteristics. These materials were then evaluated as photocatalysts for the degradation of RhB, TC, and SMX. The key findings of the study are as follows:

The BiBDC metal-organic framework (MOF), based on bismuth centers and terephthalic acid organic linkers, was successfully synthesized at various solvothermal reaction temperatures. The synthesis temperature was found to influence both the crystallinity and morphology of BiBDC. Among the different reaction temperatures, the BiBDC material synthesized at 100 °C exhibited the highest photocatalytic efficiency for RhB degradation, achieving a degradation rate of 98%. LC-MS analysis revealed that RhB degradation occurred via a carboxylation and dealkylation mechanism. The photocatalytic performance of BiBDC-100 was further optimized by evaluating the effects of catalyst dosage, dye concentration, and pH. The synthesized BiBDC MOF also demonstrated excellent stability and reusability.

The MIX-UCAU heterojunction system, combining CAU-17 and UU-200 MOFs with bismuth centers and terephthalic acid linkers, was successfully synthesized. The integration of these individual MOFs into a heterostructure improved light absorption and electron-hole separation efficiency due to the heterojunction interface between CAU-17 and UU-200. The MIX-UCAU material demonstrated enhanced photocatalytic activity, with RhB degradation reaching 99%, outperforming the individual MOFs. Radical scavenger analysis indicated that $\bullet O_2^-$ and h^+ radicals played a significant role in the degradation of RhB. Based on the experimental findings, a degradation pathway was proposed, involving N-alkylation, decarboxylation, and ring cleavage, followed by mineralization to CO_2 and H_2O. The MIX-UCAU material also exhibited good stability and reusability.

The CAU-17/BiOCl heterojunction system was successfully synthesized using a thin-film synthesis method to directly grow CAU-17 on flower-like BiOCl nanoplates. This study demonstrated the effective combination of inorganic and organic materials through a simple synthesis process. The 12h-CAU-17/BiOCl material, used as a photocatalyst, achieved 96% RhB degradation and 78.4% TC degradation. The enhanced performance was attributed to the improved visible light absorption of BiOCl, the additional reaction sites provided by the thin CAU-17 layers, and charge separation through the S-scheme heterojunction mechanism between CAU-17 and BiOCl. This mechanism facilitated the separation of electrons (e^-) and holes (h^+) upon light excitation.

The BiOCl/BHP composite, consisting of bismuth oxychloride and bismuth halide perovskite nanoplates derived from the CAU-17 MOF, was successfully synthesized. The 8h-BiOCl/BHP material, optimized for photocatalytic applications, achieved RhB degradation of 99.8% and SMX degradation of 75.1%. The enhanced photocatalytic performance was attributed to the in-situ formation of BiOCl/BHP components from CAU-17, which effectively prevented the aggregation of BHP and pure BiOCl particles. The BiOCl/BHP composite formed a surface connection between the two materials, promoting efficient charge separation and transfer pathways and improving light absorption through the S-scheme heterostructure mechanism.

DRAFT

RECOMMENDATIONS

The development of BiBDC, CAU-17, UU-200, MIX-UCAU, CAU-17/BiOCl, and BiOCl/BHP materials presents significant potential for photocatalytic applications, particularly in the simultaneous degradation of various organic pollutants in water. This research focuses on advancing the synthesis and modification of Bi-MOF materials, which are based on bismuth metal centers and diverse organic linkers, to enhance their photocatalytic efficiency and broaden their applications. Future research aims to explore the synthesis of Bi-MOF composite systems, including bimetallic MOFs, metal-doped phases, and modified Bi-MOFs, to improve the photocatalytic degradation of organic pollutants.

These innovative Bi-MOF materials and composites are expected to be applied in the degradation of a wide range of organic pollutants, such as dyes, pharmaceuticals, and pesticides, offering sustainable solutions for environmental remediation. In addition to their use in photocatalysis, these materials hold promise for various other applications, including energy production, environmental monitoring, and the development of advanced materials for other catalytic processes. Continued exploration of Bi-MOF composites will contribute to the optimization of photocatalytic processes, enhance their stability and reusability, and provide valuable insights into the mechanisms underlying efficient pollutant degradation.

DRAFT

LIST OF PUBLICATIONS RELATED TO THE DISSERTATION

I. International Journal

1. **Hoang Ai Le Pham**, The Ky Vo, Duy Trinh Nguyen, Huu Khanh Huynh, Quynh Thai Son Pham, Van Cuong Nguyen. (2022). ***Facile synthesis of bismuth terephthalate metal–organic frameworks and their visible-light-driven photocatalytic activities toward Rhodamine B dye***. Green Chemistry Letters and Reviews (ISSN: 1751-7192), Volume 15, 202- Issue 3, Pages 572-581. https://doi.org/10.1080/17518253.2022.2117998. (Q1, IF = 6.6)

2. **Hoang Ai Le Pham**, Ammar Ali Abd, Hong Anh Nguyen , Ngoc Bao Tran Le, Trinh Duy Nguyen, Van Cuong Nguyen, Mohd Roslee Othman. (2023). ***Optimization of photocatalytic degradation performance of organic dye using highly efficient bismuth MOFs: Preparation and parametric analysis.*** Chemical Engineering Research and Design, 198, 196–207. https://doi.org/10.1016/j.cherd.2023.08.040. (Q2, IF = 3.7)

3. **Hoang Ai Le Pham** , Duy Trinh Nguyen, Van Cuong Nguyen , The Ky Vo. (2023). ***Integrating Bi-containing metal–organic frameworks for enhancing their LED visible-light-driven photocatalytic activities towards Rhodamine dye***. Inorganic Chemistry Communications, 159. https://doi.org/10.1016/j.inoche.2023.111822. (Q2, IF = 4.4)

4. **Hoang Ai Le Pham**, Vinh Huu Nguyen , Taeyoon Lee, Van Cuong Nguyen, Trinh Duy Nguyen. (2024). ***Construction of BiOCl/bismuth-based halide perovskite heterojunctions derived from the metal-organic framework CAU-17 for effective photocatalytic degradation.*** Chemosphere, 357(February), 142114. https://doi.org/10.1016/j.chemosphere.2024.142114. (Q1, IF = 8.1)

5. Vinh Huu Nguyen, **Hoang Ai Le Pham**, Taeyoon Lee, Trinh Duy Nguyen. (2024). ***Synthesis of a 3D Flower-Like BiOCl/Bi-MOF Heterostructure for High-Performance Removal of Rhodamine B and Tetracycline Hydrochloride***, Inorg Chem, 2024, doi: 10.1021/acs.inorgchem.4c00877. (Q1, IF= 4.3)

II. Domestic Journals

6. **Phạm Hoàng Ái Lệ,** Nguyễn Duy Thanh, Lê Hoài Ân, Nguyễn Duy Trinh, Nguyễn Văn Cường. (2024). **"Synthesis of bismuth metal-organic frameworks and trimesic acid with different solvent systems and their application as photocatalysts for the degradation of Rhodamine B dye in water,"** *Vietnam Journal of Catalysis and Adsorption*.

III. Conferences

1. **Phạm Hoàng Ái Lệ** (2024). ***Synthesis of Metal-Organic Framework of bismuth and trimesic acid under different solvent systems and application as photocatalyst for treatment of Rhodamine B dye***, The 12th Vietnam National Conference on Catalysis and Adsorption, catasysis and adsorption in the face of energy transition challenges. Date 23-25/5/2014, Petrovietnam University.

2. **Phạm Hoàng Ái Lệ (2024). "Synthesis of Bismuth Trimesic Metal-Organic Framework and Its Application for Rhodamine Dye Treatment in Water," Scientific Workshop: Electrochemical Applications in Pharmaceutical Analysis.** Date: May 22, 2024, Industrial University of Ho Chi Minh City

3**. Phạm Hoàng Ái Lệ,** Nguyễn Thị Huệ, Nguyễn Duy Trinh. (2021). ***Research on synthetic metal frame materials with different metal and application in organic color dispatching***. Abstract book of the 3rd Young Scientists Conference (YSC 2021), Industrial University of Ho Chi Minh City.

DRAFT